Molecular Plant
Research article

CellPress
Partner Journal

Hordedane diterpenoid phytoalexins restrict *Fusarium graminearum* infection but enhance *Bipolaris sorokiniana* colonization of barley roots

Yaming Liu[1], Dario Esposto[1], Lisa K. Mahdi[2], Andrea Porzel[3], Pauline Stark[3], Hidayat Hussain[3], Anja Scherr-Henning[1], Simon Isfort[1], Ulschan. Bathe[1,5], Iván F. Acosta[4], Alga Zuccaro[2], Gerd U. Balcke[1] and Alain Tissier[1,*]

[1]Department of Cell and Metabolic Biology, Leibniz Institute of Plant Biochemistry, Halle, Germany

[2]Institute for Plant Sciences, Cluster of Excellence on Plant Sciences (CEPLAS), Cologne Biocenter, University of Cologne, Cologne, Germany

[3]Department of Bioorganic Chemistry, Leibniz Institute of Plant Biochemistry, Halle, Germany

[4]Max Planck Institute for Plant Breeding Research, Cologne, Germany

[5]Present address: Horticultural Sciences, University of Florida, Gainesville, FL, USA.

***Correspondence: Alain Tissier (alain.tissier@ipb-halle.de)**

https://doi.org/10.1016/j.molp.2024.07.006

ABSTRACT

Plant immunity is a multilayered process that includes recognition of patterns or effectors from pathogens to elicit defense responses. These include the induction of a cocktail of defense metabolites that typically restrict pathogen virulence. Here, we investigate the interaction between barley roots and the fungal pathogens *Bipolaris sorokiniana* (*Bs*) and *Fusarium graminearum* (*Fg*) at the metabolite level. We identify hordedanes, a previously undescribed set of labdane-related diterpenoids with antimicrobial properties, as critical players in these interactions. Infection of barley roots by *Bs* and *Fg* elicits hordedane synthesis from a 600-kb gene cluster. Heterologous reconstruction of the biosynthesis pathway in yeast and *Nicotiana benthamiana* produced several hordedanes, including one of the most functionally decorated products 19-β-hydroxy-hordetrienoic acid (19-OH-HTA). Barley mutants in the diterpene synthase genes of this cluster are unable to produce hordedanes but, unexpectedly, show reduced *Bs* colonization. By contrast, colonization by *Fusarium graminearum*, another fungal pathogen of barley and wheat, is 4-fold higher in the mutants completely lacking hordedanes. Accordingly, 19-OH-HTA enhances both germination and growth of *Bs*, whereas it inhibits other pathogenic fungi, including *Fg*. Analysis of microscopy and transcriptomics data suggest that hordedanes delay the necrotrophic phase of *Bs*. Taken together, these results show that adapted pathogens such as *Bs* can subvert plant metabolic defenses to facilitate root colonization.

Keywords: barley, *Hordeum vulgare*, diterpenoid phytoalexins, gene cluster, pathogenic fungi, *Bipolaris sorokiniana*, *Fusarium graminearum*

Liu Y., Esposto D., Mahdi L.K., Porzel A., Stark P., Hussain H., Scherr-Henning A., Isfort S., Bathe Ulschan., Acosta I.F., Zuccaro A., Balcke G.U., and Tissier A. (2024). Hordedane diterpenoid phytoalexins restrict *Fusarium graminearum* infection but enhance *Bipolaris sorokiniana* colonization of barley roots. Mol. Plant. **17**, 1307–1327.

INTRODUCTION

Plant pathogenic fungi impose a major burden on crop yield, and this impact is expected to increase with climate change (Miedaner and Juroszek, 2021). As the use of agrochemicals is increasingly under scrutiny by environmental agencies and single gene-for-gene resistance can be rapidly overcome in a changing environment, there is a strong need for more durable resistance traits. The fungus *Bipolaris sorokiniana* (*Bs*, teleomorph *Cochliobolus sativus*) is the pathogenic agent of spot blotch and root rot in wheat and barley and is particularly prevalent in regions with warmer climates (Rosyara et al., 2010). Therefore, it represents a typical future important threat in the context of global warming. *Bs* can infect both aerial and underground parts of the plant, but

Published by the Molecular Plant Shanghai Editorial Office in association with Cell Press, an imprint of Elsevier Inc., on behalf of CSPB and CEMPS, CAS.

knowledge on how it interacts with roots is still limited (Sarkar et al., 2019).

The interaction of plants with pathogens is a complex process that involves multiple molecular mechanisms and varies depending on the species involved. A first level is the recognition of pathogen- or microbial-associated molecular patterns (PAMPs or MAMPs) present at the surface of pathogens that are recognized by membrane receptors (pattern recognition receptors) to trigger immunity. Additionally, degradation products of the cell wall (damage-associated molecular patterns [DAMPs]), either of the pathogen or of the plant, can also elicit immune responses. This type of defense is called pattern-triggered immunity (PTI). Pathogens use multiple effectors to manipulate the host for their own purpose, for example, to release sugars or to weaken the defense responses (Toruño et al., 2016). Effectors are typically proteins that are secreted in the apoplast or even injected into the host cells. Through the specific recognition of these effectors by receptors that locate either at the surface or inside the cells, depending on where the recognized effector is present, plants have evolved a second layer of resistance. This is the basis for the ''gene-for-gene'' model of resistance, whereby products of an avirulence gene from a pathogen, actually encoding a virulence factor (or effector), are specifically recognized by an immune receptor of the host encoded by an *R* gene. Although there are different types of *R* genes, many encode nucleotide-binding, leucine-rich repeat proteins. This effector-triggered immunity (ETI) can be rapidly overcome when pathogens evolve effectors that are not bound any longer by these receptors, a phenomenon that has led to the formulation of the ''zig-zag model'' of the evolution of plant resistance (Jones and Dangl, 2006; Jones et al., 2024). ETI typically leads to a hypersensitive response, with rapid cell death at the infection site preventing propagation of the pathogen. By contrast, PTI rather induces responses that entail the production of defense metabolites. This is in fact how the first PAMP was discovered, by purifying a peptide (Pep13) that could elicit the production of antimicrobial phenolic compounds in parsley cells (Nürnberger et al., 1994). These induced defense metabolites are called phytoalexins and are not restricted to a particular chemical class but belong, for example, to phenylpropanoids, alkaloids, or terpenoids (Ahuja et al., 2012). In barley, there are several reports of various phytoalexins produced in response to diverse pathogens. These include phenylamides, such as the dimeric hordatine A and B, the indole-derived gramine, benzoxazinones such as 2,4-dihydroxy-1,4-benzoxazin-3-one (DIBOA), and methoxychalcones, as well as tyramine and related amines (Ishihara et al., 2017; Ube et al., 2017, 2021). There are also extensive data on the nature and biosynthesis of a range of terpenoid phytoalexins in other important grass crops. Rice produces several classes of labdane-related diterpenoids, including momilactones (A and B) (Kato et al., 1973; Cartwright et al., 1977), phytocassanes, oryzalexins (Akatsuka et al., 1983; Kono et al., 1984; Sekido et al., 1986; Kato et al., 1993, 1994), and oryzalides (Watanabe et al., 1990; Kono et al., 1991), and the macrocyclic *ent*-oxodepressin (Inoue et al., 2013). Maize produces dolabralexins and kauralexins, both labdane-related diterpenoid phytoalexins (Schmelz et al., 2011), as well as the sesquiterpenoid zealexins (Huffaker et al., 2011).

Several functions and activities have been reported for these terpenoids in rice and maize. For example, the production of rice diterpenoids is induced upon exposure to pathogens such as *Magnaporthe oryzae* or *Xanthomonas oryzae*, and inhibition of spore germination and hyphal growth of *M. oryzae* was shown for momilactones A and B (Cartwright et al., 1977), oryzalexins (Akatsuka et al., 1983; Sekido et al., 1986; Kato et al., 1993, 1994), or phytocassanes (Koga et al., 1997). Momilactones A and B were originally discovered as inhibitors of root growth (Kato et al., 1973) and subsequently found to be secreted by rice roots, with momilactone B having strong allelopathic activity (Kato-Noguchi et al., 2002; Kato-Noguchi and Ino, 2003). Similarly, zealexins and kauralexins, maize terpenoid phytoalexins, are strongly induced by various fungal pathogens and have antifungal activity (Huffaker et al., 2011; Schmelz et al., 2011).

Recent years have witnessed great progress in the elucidation of the biosynthesis of these monocot terpenoid phytoalexins (Schmelz et al., 2014; Block et al., 2019; Murphy and Zerbe, 2020). While sesquiterpenoids typically derive from cytosolic isoprenyl precursors produced via the mevalonate pathway, diterpenoids generally originate from the plastidial precursors provided by the methylerythritol phosphate pathway. Most of the rice and maize diterpenoids, except the rice oxodepressin, are labdane-related, and the synthesis of their backbone occurs in two steps, first by a copalyl diphosphate synthase (CPS) followed by a kaurene synthase-like (KSL). In rice, both OsCPS1 and OsCPS2 synthesize *ent*-copalyl diphosphate (*ent*-CDP); however, OsCPS1 supplies *ent*-CDP for gibberellins, whereas OsCPS2 does it for phytocassanes and oryzalexins A–F (Otomo et al., 2004a; Prisic et al., 2004; Toyomasu et al., 2015). The momilactones are derived from *syn*-CDP, which is synthesized by OsCPS4 (Otomo et al., 2004a). Rice possesses several KSL-encoding genes, each with a specific product profile that supplies precursors for distinct classes of diterpenoid phytoalexins (Toyomasu et al., 2020). For example, OsKSL4 produces *syn*-pimara-7,15-diene, the precursor of momilactones (Otomo et al., 2004b; Wilderman et al., 2004), while the product of OsKSL7 is *ent*-cassa-7,12-diene, the precursor of phytocassanes (Cho et al., 2004). Functionalization of the diterpene backbone is typically carried out by cytochrome P450 oxygenases (CYPs), although other types of oxidoreductases can also be involved. For example, the biosynthesis of momilactones A and B was completely solved and reconstituted in *Nicotiana benthamiana*, requiring the activity of four different CYPs (CYP76M8, CYP76M14, CYP99A3, and CYP701A8) and a short-chain dehydrogenase reductase (Shimura et al., 2007; Wang et al., 2011, 2012a; Kitaoka et al., 2015; De La Peña and Sattely, 2021). Biosynthesis of the maize kauralexins follows a similar pattern, with involvement of *ent*-CPS (ZmAN2), KSLs (ZmKSL4 and ZmKSL2), CYPs (CYP71Z16/18 and kaurene oxidase-like), as well as a reductase (Harris et al., 2005; Vaughan et al., 2015; Fu et al., 2016; Ding et al., 2019). Intriguingly, some of the CYPs (CYP71Z16/18) are also involved in the biosynthesis of the zealexins, which are sesquiterpenoid phytoalexins (Ding et al., 2020), underscoring the importance of substrate promiscuity in plant specialized metabolism.

The knowledge of the genes involved in these pathways allows the investigation of the functions of the diterpenoid phytoalexins

in planta by analysis of mutants impaired in their biosynthesis. For example, mutations in *ZmAN2*, which prevent the production of both kauralexins and dolabralexins, result in increased sensitivity to fungal pathogens (Christensen et al., 2018). Mutations in *ZmKSL2* leading to the absence of only kauralexins also confer decreased resistance to *Fusarium graminearum* (*Fg*) (Ding et al., 2019). Similar observations were made in rice, with mutants in *OsCPS4* deficient in the production of momilactones and oryzalectin S being more sensitive to rice blast fungus (Toyomasu et al., 2014). The exudation by roots of diterpenoid phytoalexins suggests a role in the interaction with soil microorganisms. Indeed, the absence of diterpenoid phytoalexins leads to changes in the microbiome composition of the rhizosphere, although the biological significance of these changes is not clear (Murphy et al., 2021). Furthermore, the implications of terpenoid phytoalexins in the defense against nematodes or insects could reflect a general toxicity of these compounds (Desmedt et al., 2022). Also noteworthy is the induction of some of these diterpenoid phytoalexins by abiotic stresses, such as UV irradiation or drought, as in switchgrass and maize (Vaughan et al., 2015; Tiedge et al., 2022). Interestingly, rice *cps2*/*cps4* double mutants are more sensitive to drought, and it was proposed that rice diterpenoid phytoalexins are involved in the closure of stomata to restrict pathogen entry (Zhang et al., 2021).

Although there is evidence that diterpenoid phytoalexin biosynthesis is also present in the Pooideae clade of the grasses, which includes the major temperate cereal crops such as wheat, barley, rye, and oats, there is little information so far on the biosynthesis of these compounds, except the characterization of diterpene synthases (Wu et al., 2012; Zhou et al., 2012; Liang et al., 2022). It has been speculated that the gene-for-gene model is not the dominant system in the interaction between barley and *Bs* (Ghazvini and Tekauz, 2008). Therefore, it is important to understand the metabolic defenses of barley that can contribute to a more durable resistance.

Here, we characterize a barley gene cluster responsible for the production of a set of diterpenoid phytoalexins and investigate their role during the interaction with *Bs*. Unexpectedly, we find that *Bs* colonization of gene-edited barley mutants that do not produce these diterpenoids is less effective than that of wild-type (WT) plants. In agreement with this colonization phenotype, *Bs* grows faster in the presence of a major barley diterpenoid and displays the ability to modify it, providing an explanation for the enhanced colonization when these phytoalexins are produced.

RESULTS

A barley gene cluster for the biosynthesis of diterpenoid phytoalexins

In previous work, we identified a set of genes induced upon infection with *Bs* potentially involved in diterpenoid biosynthesis, including homologs of a copalyl diphosphate synthase (*HvCPS2*), a KSL (*HvKSL4*), and several CYPs (Sarkar et al., 2019) (Figure 1A). These genes are clustered on chromosome 2 in a region spanning around 600 kb (Figure 1A and Supplemental Table 1). A phylogenetic analysis of the encoded proteins suggests that HvCPS2 is a (+)-copalyl diphosphate synthase and shows that the CYPs from the cluster belong to two families, respectively CYP99A and CYP89E (Figure 1, Supplemental Figures 1 and 2, and Supplemental Tables 2–4). Notably, CYP99As are also found in the momilactone gene cluster in rice (Shimura et al., 2007) and in a diterpenoid gene cluster in *Setaria viridis* (Karunanithi et al., 2020). Most genes in the barley cluster show strong transcriptional induction upon infection by *Bs* (Figure 1B). Analysis of extracts from roots and root exudates by gas chromatography–mass spectrometry (GC–MS) and liquid chromatography–tandem mass spectrometry (LC–MS/MS) indicates the presence of several compounds with masses and fragmentation patterns indicative of diterpenoids (Figure 1D and Supplemental Figure 3), suggesting that they may be products of the chromosome 2 cluster.

Heterologous expression identifies a set of barley diterpenoids of the cleistanthane group

Using previously established expression systems in yeast (*Saccharomyces cerevisiae*) and *N. benthamiana* (Bruckner and Tissier, 2013; Scheler et al., 2016) as well as *in vitro* assays, we reconstituted major parts of a network of diterpenoids and characterized several of the intermediates and products by nuclear magnetic resonance (NMR). As reported previously by our group and others (Liu et al., 2021; Liang et al., 2022), the diterpene backbone (compound **1**) produced by the combined action of HvCPS2 and HvKSL4 stems from (+)-copalyl diphosphate and belongs to the cleistanthane class, with two double bonds in the C-ring at positions C8–C9 and C12–C13, a methyl group attached to C13, and an ethyl group attached to C14 in the α configuration (Supplemental Figure 4; Supplemental Data 1, **1**; Supplemental Table 5). We named this diterpene olefin hordediene and the group of barley diterpenoids derived from it hordedanes. We then expressed the four most highly expressed CYPs from the cluster (CYP89E31, CYP99A66, CYP99A67, and CYP99A68) with HvCPS2 and HvKSL4 either individually or in combinations of 2–3 CYPs. CYP89E31 carries out aromatization of the C-ring (compound **5**; Supplemental Figure 9 and Supplemental Data 1, **5**) and C11-hydroxylation (compound **8**, Supplemental Data 1, **8**), as described in our earlier preprint (Liu et al., 2021) (Figure 2A; Supplemental Figures 5 and 6; Supplemental Tables 6 and 7). Both **5** and **8** are present in barley root extracts elicited by *Bs* infection (Supplemental Figure 3). CYP99A66 and CYP99A67 have partially overlapping activities with both able to oxidize the C17-methyl group multiple times, while only CYP99A67 is able to oxidize the C19-methyl group (Figure 2A–2C; Supplemental Figures 5 and 7; Supplemental Data 1, **18**–**20**; Supplemental Table 9). CYP99A68 oxidizes compound **8** multiple times on C16, leading to compound **22**, which is present in *Bs*-infected roots and root exudates (Figure 2C, Supplemental Figure 8, and Supplemental Data 1, **21**–**24**). In total, we detected at least 17 hordedanes in barley roots, of which nine were produced in yeast (Figure 2A).

Importantly, the combination of CYP89E31, CYP99A66, and CYP99A67 with HvCPS2 and HvKSL4 results in the production of compounds **21a** and **21b**, respectively, 19-β-hydroxy-hordetrien-17-oic acid (19-OH-HTA), and 3-β-hydroxy-hordetrien-17-oic acid (3-OH-HTA), which combined represent the most abundant peak (**21**) in barley root exudates, albeit in a different ratio

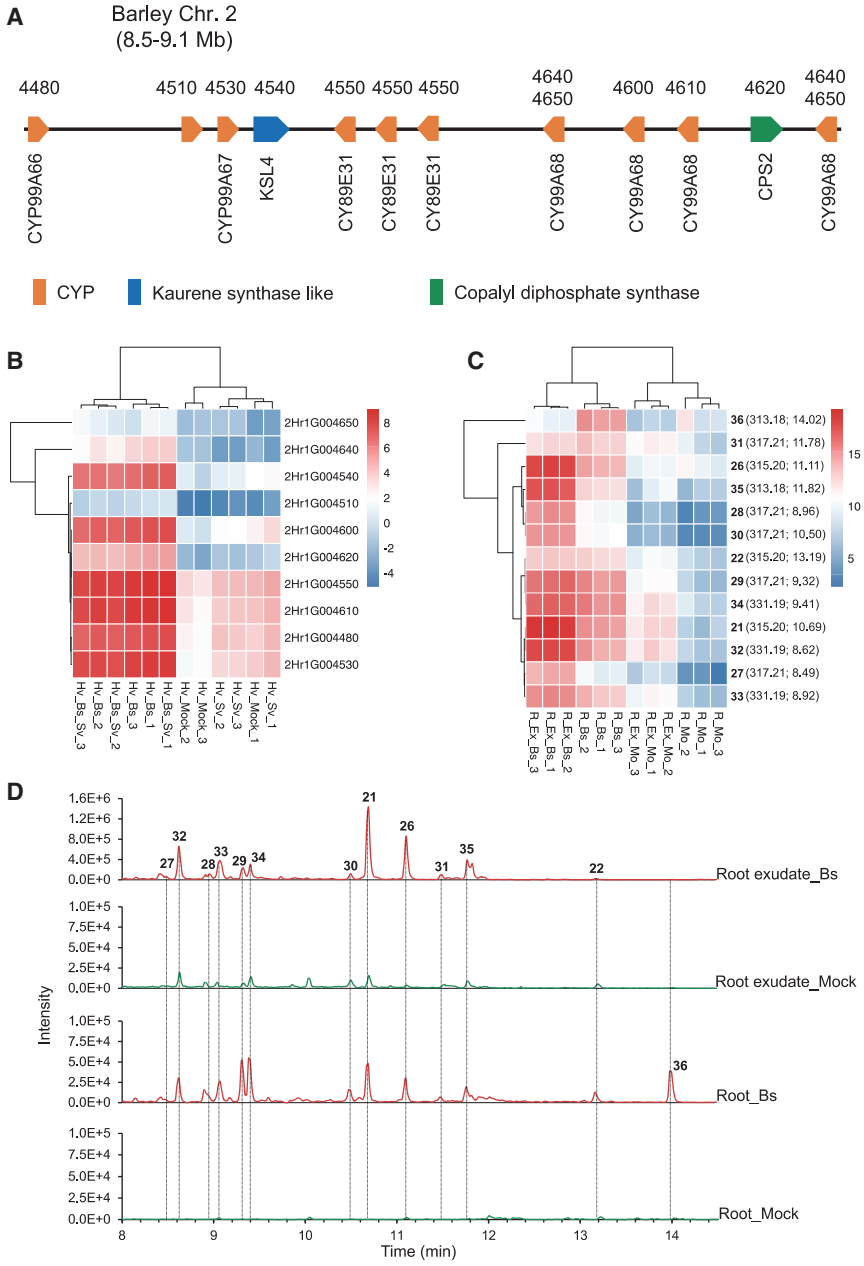

Figure 1. Pathogen-inducible expression of a barley gene cluster for diterpenoid biosynthesis and production of diterpenoids upon pathogen infection of barley roots.

(A) Overview of the chromosome 2 biosynthetic gene cluster. Three versions of the barley reference genome, Morex V1, V2, and V3 (Beier et al., 2017; Monat et al., 2019; Mascher et al., 2021), were used to generate the gene annotation. The number on the top of genes indicates the last four digits of the gene ID according to Morex V1, and the given name of the genes is provided below. CYP, cytochrome P450 oxygenase; Mb, million base pairs.

(B) Differential expression of genes from the cluster upon infection of barley roots by pathogenic and beneficial endophytic fungi. The colors represent gene expression values as log_2-transformed FPKM values (fragments per kilobase per million mapped reads). The raw data are from (Sarkar et al., 2019). Hv_Mock, barley roots mock inoculated; Hv_Sv; barley roots inoculated with *Serendipita vermifera* (*Sv*); Hv_Bs, barley roots inoculated with *Bipolaris sorokiniana* (*Bs*); Hv_Bs_Sv, barley roots co-inoculated with *Bs* and *Sv*.

(C) Diterpenoids identified from barley roots or root exudates after *Bs* infection and compared with mock-treated samples. R_Bs, roots inoculated with *Bs*; R_Mo, roots mock inoculated; R_Ex_Bs, exudates of roots inoculated with *Bs*; R_Ex_Mo, exudates of roots mock inoculated. The digits at the end of the sample names indicate independent biological replicates. The color scale bar represents log_2-transformed peak intensity values measured by UPLC–quadrupole time-of-flight. The identity of each diterpenoid is indicated by a number in bold, followed by its retention time and mass-to-charge ratio.

(D) LC–high-resolution mass spectrometry (HRMS) (negative mode) chromatograms of diterpenoids from barley roots or root exudates after *Bs* infection or mock treatment. Selected ions: *m/z* 313.2, 315.2, 317.2, and 331.2.

in yeast and barley (Figure 2C; Supplemental Figure 10; Supplemental Data 1, **21**; Supplemental Table 10). These results show that we could reconstitute to a large extent the pathway for the barley diterpenoid phytoalexins in yeast.

Hordedane diterpenoids are absent in *Hvcps2* and *Hvksl4* mutants

To evaluate the contribution of *HvCPS2* and *HvKSL4* to the barley diterpenoids and to study their biological roles in the interaction with *Bs*, we performed targeted mutagenesis of *HvCPS2* and *HvKSL4* by CRISPR/Cas9-mediated gene editing on the barley cultivar Golden Promise Fast, hereafter referred to as WT (Gol et al., 2021). Two single-guide RNAs (sgRNAs) for each gene were used, and two independent homozygous mutant lines for both *HvCPS2* and *HvKSL4* (*Hvcps2.1*, *Hvcps2.2*, *Hvksl4.1*, and *Hvksl4.2*) were selected for further characterization (Supplemental Figure 11). All mutations lead to a premature stop codon and the synthesis of truncated proteins missing essential residues for catalysis (Supplemental Figure 11B and 11C). Furthermore, the expression of the mutated genes is strongly reduced in the respective mutants (Supplemental Figure 12). We performed an infection assay with *Bs* on the four mutants and WT barley and analyzed roots and root exudates by untargeted metabolomic profiling. The induced diterpenoids in WT plants are absent in all four mutants (Figure 3A). These results show that these diterpenoids are derived from the products of the two diterpene synthases encoded by *HvCPS2* and *HvKSL4* in the chromosome 2 gene cluster. However, only in the *Hvksl4* mutants, we observed the presence of diterpenoids with masses

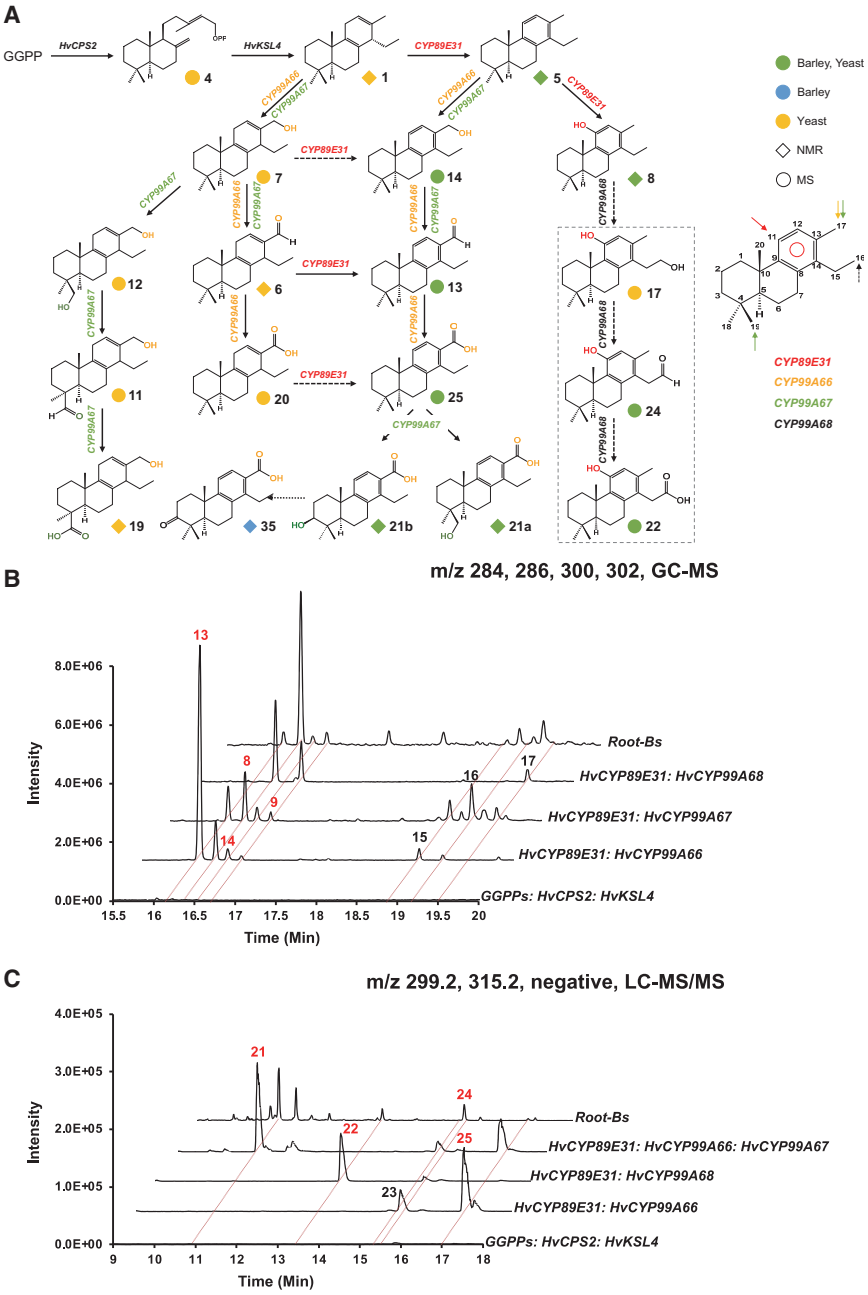

Figure 2. Elucidation of the biosynthetic pathway of barley diterpenoids.

(A) Biosynthesis pathway of barley diterpenoids by heterologous expression in yeast and *N. benthamiana*. The diamond and the circle symbols indicate diterpenoids characterized by NMR and MS, respectively. Green symbols indicate diterpenoids identified in barley, yeast, and *N. benthamiana*. Blue symbols indicate diterpenoids identified in barley only; orange symbols indicate diterpenoids identified only in heterologous expression.

(B and C) GC–MS **(B)** or LC–MS/MS **(C)** analysis of diterpenoid products from heterologous expression in yeast of two or three *CYP*s. *CYP*s were always co-expressed together with *HvCPS2*, *HvKSL4*, and *GGPPS*. Peaks that are present in barley are indicated by red numbers.

of 320 and 336 (Figure 3B). Since HvCPS2 is still functional and expressed in *Hvksl4* mutants, (+)-copalyl diphosphate will be produced and dephosphorylated to (+)-copalol. Given the known promiscuity of CYPs, it is likely that some of the CYPs of the chromosome 2 cluster will also accept (+)-copalol as substrate and oxidize it. The observed masses indicate the presence of a hydroxyl and a carbonyl group or of a carboxylic acid (320) and of an additional hydroxyl group (336) (Supplemental Data 1, **44**–**48**).

19-OH-HTA has antifungal activity against *Fusarium* sp. and *Serendipita* sp. but enhances *Bs* growth

We took advantage of the availability of a yeast strain producing 19-OH-HTA and small amounts of 3-OH-HTA to purify the mixture and use it for bioassays. Because 19-OH-HTA is the major compound of this mixture, we refer to it as 19-OH-HTA for simplification. We tested 19-OH-HTA on five fungi, including three phytopathogens, *Bs*, *Verticilium dahliae* (*Vd*), *Fusarium graminearum* (*Fg*)—the causal agent of fusarium head blight in barley and wheat—and two beneficial fungal endophytes, *Serendipita indica* (*Si*) and *Serendipita vermifera* (*Sv*). 19-OH-HTA strongly inhibited the spore germination of *Fg* (5.2% spore germination in the presence of 19-OH-HTA versus 93.7% without it) and reduced its hyphal growth significantly (Figure 4A and 4B). Similar inhibitory effects were also observed on the two beneficial fungal endophytes, indicating a broad activity spectrum, a feature frequently reported for other phytoalexins (Huffaker et al., 2011; Schmelz et al., 2011). No effect was observed on the germination and growth of *Vd*. By contrast, 19-OH-HTA slightly enhanced the spore germination of *Bs* (Figure 4B). Furthermore, incubation with 19-OH-HTA at 1–10 μM concentrations leads to significantly enhanced growth of *Bs* in a concentration-dependent manner (Figure 4C).

Reduced root colonization of *Hvcps2* and *Hvksl4* mutants by *Bs*

Next, we compared the performance of hordedane-less barley mutants with WT plants upon infection by *Bs* and by *Fg*. We measured the fresh weight of roots at 6 days post infection (dpi) for plants infected by *Bs* and non-infected plants. Infection by *Bs* leads to growth reduction in all genotypes, but we observed no significant difference in the extent of growth reduction of roots between WT and *Hvcps2* or *Hvksl4* mutants (two-way ANOVA, $p = 0.1197$) (Supplemental Figures 13 and 14). We then quantified the relative amount of *Bs* and *Fg* in the roots of all

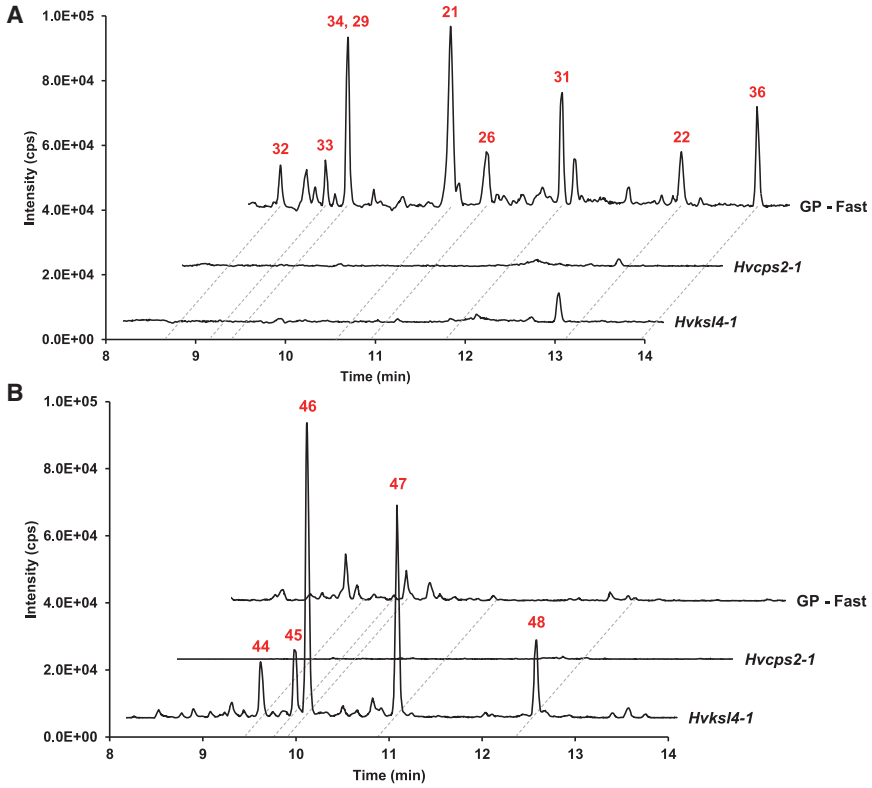

Figure 3. Characterization of barley *Hvcps2* and *Hvksl4* mutants.

(A) Chromatograms (LC–MS/MS, negative mode) of diterpenoids from roots of WT barley and *Hvcps2* and *Hvksl4* mutants after *Bs* infection. Selected ions: *m/z* 313.2, 315.2, 317.2, 331.2. These masses correspond to the hordedanes produced by barley roots upon infection by *Bs*.

(B) Same as **(A)** but from root exudates and with selected ions 319.2 and 335.2. These masses correspond to (+)-copalol derivatives that are only produced in *Hvksl4* mutants. The numbers indicate individual compounds, whose mass spectrum is shown in the supplemental figures.

genotypes by RT–qPCR. Unexpectedly, we detected less *Bs* in all four mutants compared with the WT (Figure 5A). The reduced *Bs* colonization was confirmed by measuring fluorescence after staining with a fungal-specific fluorescent marker (Figure 5B). By contrast, *Fg* fungal colonization was increased by up to almost 4-fold in *Hvcps2* mutants compared to WT, but not in *Hvksl4* mutants (Figure 5C). The latter observation can be accounted for by the presence of the oxidized copalol derivatives present only in *Hvksl4* mutants (Figure 3B). These results demonstrate the importance of barley hordedanes in contributing to resistance against *Fg* but suggest that in the context of the interaction between the pathogenic *Bs* and barley roots, the presence of the induced barley diterpenoids increases the ability of *Bs* to colonize barley roots. We therefore sought to further investigate the effect of the diterpenoids on *Bs*.

19-OH-HTA reverses the reduced colonization of diterpenoid-free mutants

We first tested the ability of 19-OH-HTA to reverse the reduced colonization of *Hvksl4* mutants. To this end, we added yeast extracts containing 19-OH-HTA at a concentration of 10 μM to the agar medium used for the colonization assays and compared it to a mock addition or to an extract from the background yeast strain, i.e., processed in the same way as for the purification of 19-OH-HTA. Quantification of *Bs* abundance by RT–qPCR shows that colonization levels were restored to WT levels in the presence of 19-OH-HTA (Figure 5D).

Barley diterpenoids are modified by *Bs*

To further investigate the growth- and colonizing-enhancing effect of 19-OH-HTA on *Bs*, we performed metabolite profiling of axenic *Bs* cultures in the presence of 19-OH-HTA. Untargeted profiling by LC–MS/MS (negative mode) of the whole culture revealed two independent modifications of 19-OH-HTA. The first pathway is through oxidation, resulting in two metabolites with *m/z* of 331 (compound **37**) and 329 (compound **38**), indicating the addition of a hydroxyl group (*m/z* 331) or further oxidation to an aldehyde or a ketone (*m/z* 329) (Figure 6A and Supplemental Data 1, **37** and **38**). We also identified a group of metabolites with *m/z* of 549 (compounds **39**, **40**, **41**, and **42**). Their mass spectra indicate that they are conjugates of 19-OH-HTA and a metabolite with mass of 252 (Figure 6B). Upon negative electrospray ionization (ESI), we detect several peaks with an *m/z* of 251, and one of them (compound **43**) was identified as helminthosporic acid by NMR (Supplemental Table 13), in agreement with published data (Miyazaki et al., 2017; Phan et al., 2019; Li et al., 2020). Helminthosporic acid is a major sesquiterpenoid metabolite isolated from *Bs* (Li et al., 2020). Compound **42** was inferred to be an ester of 19-OH-HTA and helminthosporic acid or of an isomer thereof. The other three conjugates are likely to be isomers of **42**, because *Bs* extracts contain several metabolites with the mass of 252, i.e., bipolenin-type isomers of helminthosporic acid (Phan et al., 2019) that most likely can be conjugated to 19-OH-HTA as well. Importantly, the two oxidized diterpenoids and the conjugates are present in the exudates of barley roots infected with *Bs* (Figure 6A), providing evidence that the same modifications of 19-OH-HTA occur during the interaction of barley roots with *Bs*. Notably, during a time-course experiment, the appearance of the derivatives of 19-OH-HTA coincided with the enhancement of growth of *Bs* compared to the control (Supplemental Figure 15).

Analysis of microscopy and transcriptomic data suggest that hordedanes delay the necrotrophic phase of *Bs*

To dig deeper into the interaction between *Bs* and barley diterpenoids, we first performed detailed microscopy observations at two time points (3 and 6 dpi) upon infection of barley WT and *Hvcps2* mutants by *Bs*. In cross-sections of roots, we noticed that at 3 dpi roots of *Hvcps2* mutants showed significant alteration

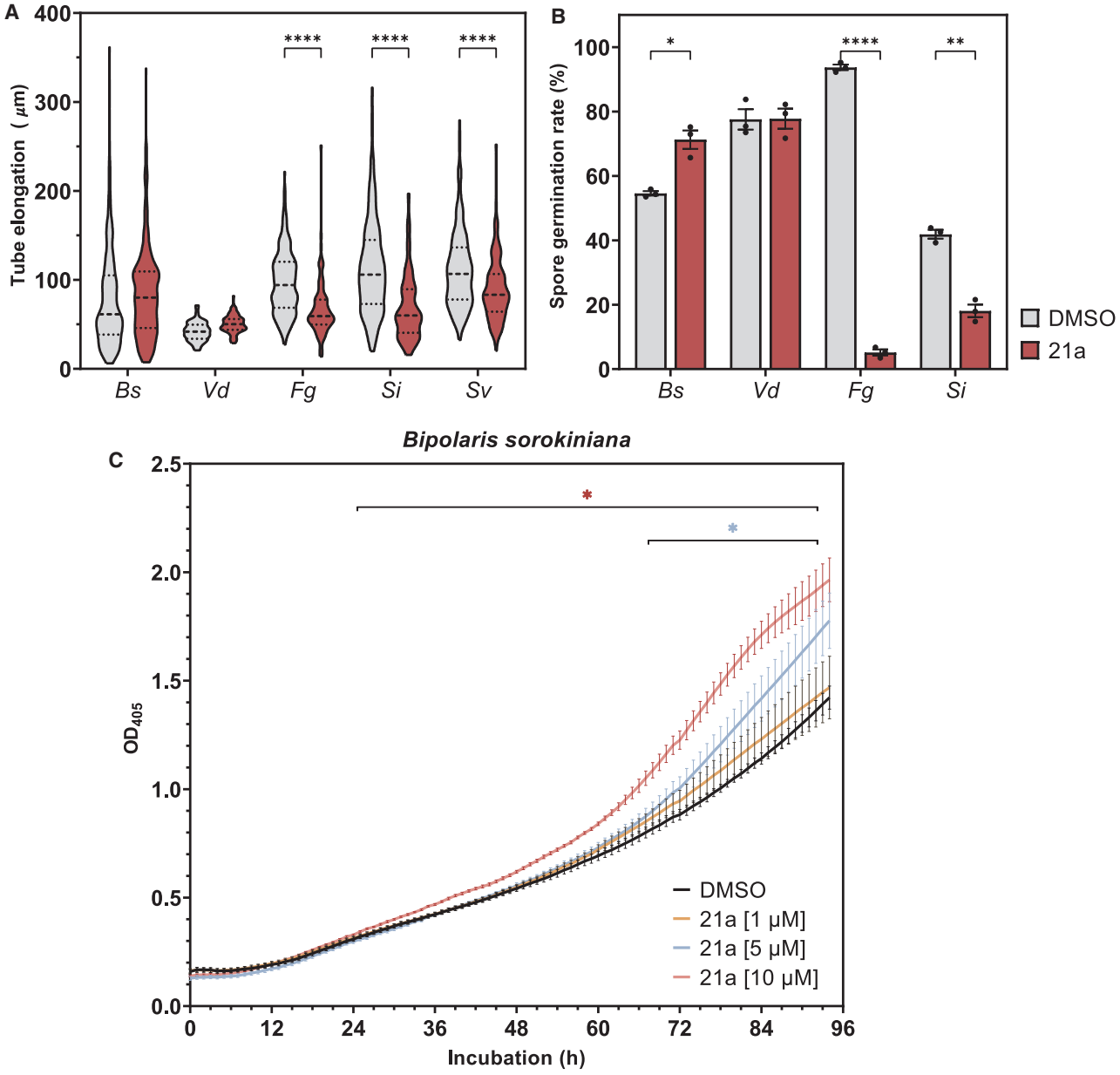

Figure 4. Effects of 19-OH-HTA application on different fungi.

(A) Tube elongation/hyphal length of *Bipolaris sorokiniana* (*Bs*, 3 hpi), *Verticilium dahlia* (*Vd*, 9 hpi), *Fusarium graminearum* (*Fg*, 9 hpi), *Serendipita indica* (*Si*, 12 hpi), and *Serendipita vermifera* (*Sv*, 12 hpi) after application of 0 (DMSO) or 10 μM 19-OH-HTA (**21a**) to the growth media.

(B) Percentage of germinated spores of *Bs* (3 hpi), *Vd* (9 hpi), *Fc* (9 hpi), and *Si* (12 hpi) after application of 0 or 10 μM 19-OH-HTA to the growth media. The incubation time depended on the speed of fungal spore germination. Error bars: mean ± SD (n = 3).

(C) *Bs* growth time course in media containing 19-OH-HTA at the concentration of 0, 1, 5, and 10 μM, respectively. The horizontal bars indicate the time from which the difference between the growth curves with **21a** and DMSO is significant ($p < 0.05$). Error bars: mean ± SEM (n = 8–9).

Asterisks indicate significant differences between control and diterpenoid-treated samples (Student's t-test; *$p < 0.05$, **$p < 0.01$, ***$p < 0.001$).

of the outer cell layers (epidermis and subepidermal layer) whereas roots of WT plants, although well colonized, were largely intact (Figure 7A). At 6 dpi, these alterations of the outer cell layers were also visible in WT (Figure 7B and 7C). *Bs* is a hemibiotrophic pathogen that first feeds on live plant cells and then switches to a necrotrophic phase (Kumar et al., 2002). Our observations indicate that in *Hvcps2* mutants the necrotrophic phase starts earlier than in WT. To corroborate this observation with molecular data, we performed transcriptome profiling by RNA sequencing (RNA-seq) on *Bs* axenic cultures with or without 19-OH-HTA at three time points (24, 48, and 72 h). Reads were mapped to the ND90Pr v1.0 version of the *Bs* genome. We found a total of 10 183, 10 246, and 9951 genes to be expressed at 24, 48, and 72 h of culture, respectively (Supplemental Data 2). A heatmap of the 300 most variable genes shows that most of the differentially expressed genes (DEGs) are due to the growth of the culture at the different time points (Supplemental Figure 16). This was also visible in a principal component analysis plot of these 300 most

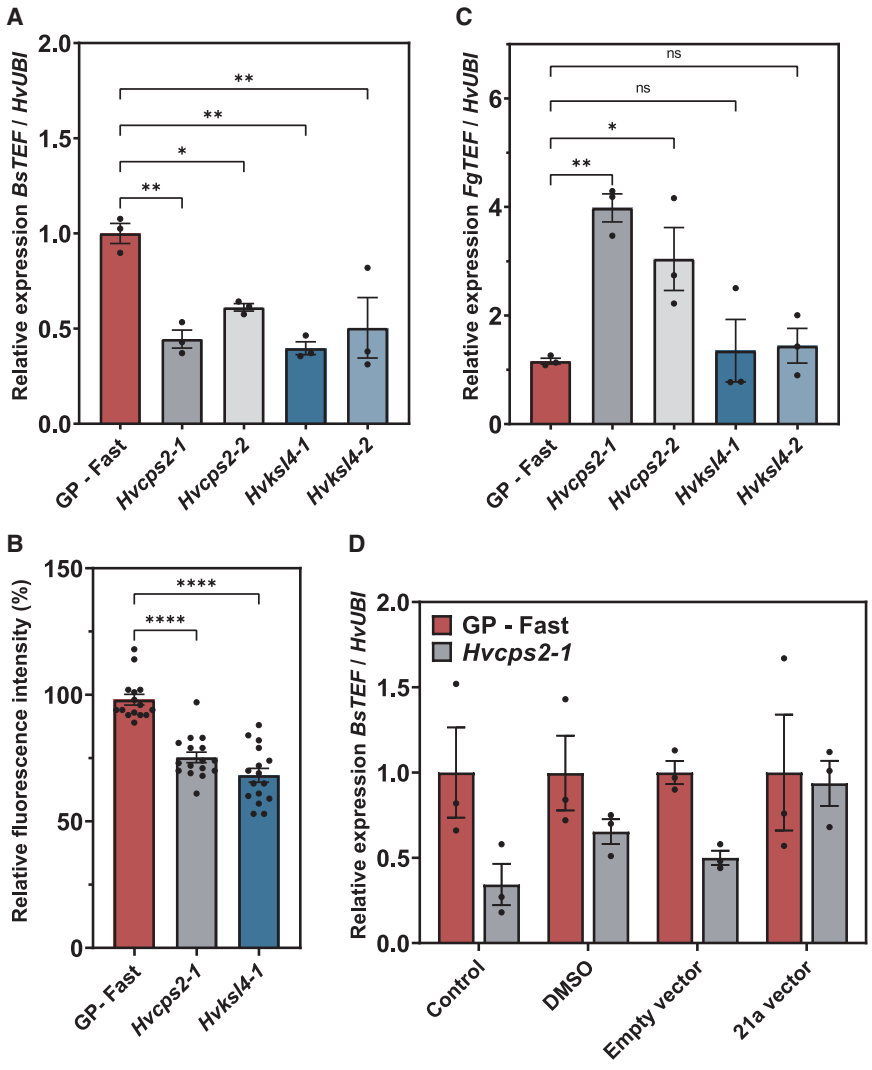

Figure 5. Colonization of WT, *Hvcps2*, and *Hvksl4* roots by *Bs* and *Fg* and complementation of *Hvcps2* mutants by 19-OH-HTA.

(A) Quantification of *Bs* in the roots by RT–qPCR at 6 dpi. Reference gene for barley: *HvUBI* (ubiquitin). Target gene for *Bs*: *BsTEF* (transcription elongation factor). Statistics: one-way ANOVA and Tukey's post hoc test, $p = 0.0039$.

(B) Quantification of barley root colonization by *Bs* at 6 dpi via fluorescence staining intensity ($n = 16$).

(C) Quantification of *Fg* in the roots by RT–qPCR at 6 dpi. Reference gene for barley: *HvUBI* (ubiquitin). Target gene for *Fg*: *FgTEF* (transcription elongation factor).

(D) Quantification of *Bs* in roots by RT–qPCR as in **(A)**. Control: control conditions, no additions to agar medium; DMSO: 2% DMSO added to upper layer of agar medium; empty vector: purified supernatant of yeast carrying an empty vector; **21a** vector: purified supernatant containing **21a** (19-OH-HTA) of yeast carrying a vector containing all genes needed to produce **21a**. Statistics: one-way ANOVA.

Error bars: mean ± SEM ($n = 3$) (*$p < 0.05$, **$p < 0.01$, ***$p < 0.001$).

variable genes (Supplemental Figure 17) showing relatively little separation of treated versus non-treated samples. We found 307 genes that showed a significant differential expression between treated and untreated samples in at least one time point ($|\log_2$ fold change$|$ $[\log_{2FC}] > 1$; $p < 0.05$) (Supplemental Data 2). Most of the genes ($n = 235$) were differentially expressed at 72 h. A selected set of DEGs with particular relevance to the interaction of *Bs* with barley is shown in Figure 7D. A gene ontology enrichment analysis of the DEGs at 24, 48, and 72 h indicate a prevalence of metabolic processes, transport processes, and oxidoreductase activity (Supplemental Figure 18), suggesting the activation of genes involved in the modification of 19-OH-HTA as observed in the LC–MS profiling (Figure 6). Potential candidate genes are, for example, several cytochrome P450 oxygenases (COCSADRAFT_202450, COCSADRAFT_46028, COCSADRAFT_188512, COCSADRAFT_197249) as well two major facilitator superfamily transporters (COCSADRAFT_183275 and COCSADRAFT_198203) that show strong induction ($\log_2$FC at 72 h >2.5) in *Bs* exposed to 19-OH-HTA (Figure 7D and Supplemental Data 2). We also observe the activation of genes potentially involved in pathogenic processes such as a glycoside hydrolyase (COCSADRAFT_41732; $\log_2$FC at 72 h = 1.8) and a peptidase (COCSADRAFT_100610; $\log_2$FC at 72 h = 2.3). Most interestingly, we noticed the downregulation of genes that are indicative of cell lytic processes. Among them are an endonuclease/exonuclease family protein (COCSADRAFT_38316; $\log_2$FC at 72 h = −2.9) and a lytic polysaccharide monooxygenase (LPMO) (COCSADRAFT_285519; $\log_2$FC at 72 h = −1.8). LPMOs in particular have greatly expanded in necrotrophic fungi and have been associated to the switch from biotrophic to necrotrophic phase of plant fungal pathogens (Jagadeeswaran et al., 2021; Vandhana et al., 2022). Both protein products of these genes are predicted to be secreted (Supplemental Data 2). Importantly, we found that the differential expression of these two genes is conserved in a previously published and independent transcriptome dataset of barley roots exposed to *Bs* and *Sv*, either alone or in combination (Figure 7D) (Sarkar et al., 2019).

Diterpenoid gene clusters are conserved in Poaceae

Similar gene clusters have been identified in rice and maize, and one would expect to find them in species more closely related to barley, such as wheat. To address this, we performed a synteny analysis of the rice, barley, and wheat genomes focusing on the barley diterpenoid cluster (Supplemental Figure 19), which shows strong conservation between the barley hordedane and the rice momilactone cluster, particularly with the presence of CPS, KSL, and CYP99 encoding genes. Interestingly, the synteny in wheat is also conserved and distributed over the three genomes (Supplemental Figure 19). The wheat clusters on the three chromosome 2 all contain a CPS and a KSL but differ in their content of CYPs, with no CYPs on chromosome 2B, and CYP99s but also CYP71s on chromosomes 2A and 2D. This analysis also revealed the presence of several glycosyltransferases, an ABC

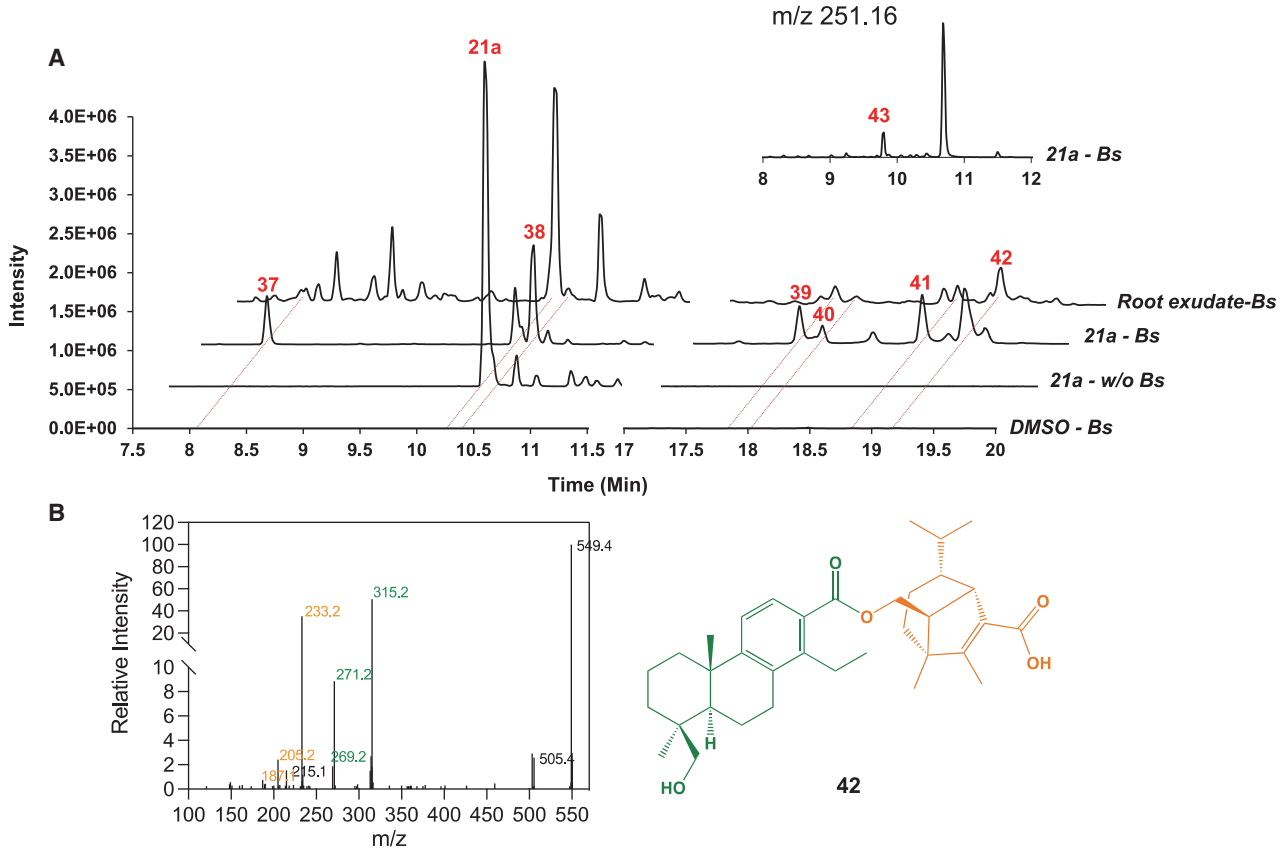

Figure 6. Metabolism of barley 19-OH-HTA by *Bipolaris sorokiniana*.
(A) LC–HRMS (negative mode) chromatogram of extracts from whole *Bs* culture or barley root exudates. *Bs* was grown in the media with or without 19-OH-HTA (**21a**), respectively, for 3 days, and a sample with **21a** at the same concentration but without *Bs* present was used as a control. All experiments were performed in triplicates and were repeated multiple times. The ions used for the extracted ion chromatograms are *m/z* 315.2, 329.2, 331.2, and 549.3. The inset shows a part of the chromatogram with ion *m/z* 251.16 selected, with the peak for compound **43** from *Bs*, which is helminthosporic acid.
(B) MS/MS spectra of **42**. The fragments putatively derived from **21a** are colored green, while those putatively derived from **43** are orange.

transporter, and a chalcone synthase. We could detect glycosylated 19-OH-HTA in barley (Supplemental Figure 20), so it is possible that some of these genes are involved in the diterpenoid pathway. Based on these data, it is likely that wheat also produces a set of diterpenoid phytoalexins. To explore this, we inoculated wheat with *Bs* and performed metabolic profiling as for barley diterpenoids. We detected several compounds whose *m/z* signals and fragmentation patterns are consistent with those of diterpenoids (Supplemental Figure 21). Diterpene synthases (a CPS and a KSL) from these clusters have been characterized and most likely provide a backbone for the diterpenoids observed (Wu et al., 2012; Zhou et al., 2012; Polturak et al., 2022). Beyond wheat, the conservation of this cluster across distant monocots such as rice, barley, and wheat, but not maize, suggests that many Poaceae are likely to contain similar clusters but produce diverse (di)terpenoids and thereby contribute to the diversity of the terpenoid chemical space.

DISCUSSION

Cleistanthane diterpenoids: A new class of plant phytoalexins produced by a biosynthetic gene cluster

Since the discovery of diterpenoid phytoalexins in rice and the elucidation of their biosynthesis, there has been an increasing number of reports on investigations of specialized diterpenoid metabolism in monocots. This includes, for example, maize (*Zea mays*) (Schmelz et al., 2011; Ding et al., 2020), switchgrass (*Panicum virgatum*) (Pelot et al., 2018; Muchlinski et al., 2021; Tiedge et al., 2022), and wheat (*Triticum aestivum*) (Wu et al., 2012; Zhou et al., 2012; Polturak et al., 2022). In the Triticeae, which comprise wheat, barley, and rye (*Secale cereale*), despite the publication of reports describing the characterization of wheat diterpene synthases (Wu et al., 2012; Zhou et al., 2012; Polturak et al., 2022), to the best of our knowledge no diterpenoid phytoalexins has yet been identified. Our work shows that like maize and rice, barley is also able to produce diterpenoid phytoalexins when challenged with a pathogen. Thus, production of diterpenoid phytoalexins appears to be a common feature of monocots. It is also noteworthy that the genes involved in the biosynthesis of these compounds are frequently localized in clusters encoding diterpene synthases (CPS and KSL) as well as CYPs or, in the case of rice, a short-chain dehydrogenase reductase (OsMAS) (Shimura et al., 2007; Ding et al., 2020; Muchlinski et al., 2021). Clusters of genes involved in specialized metabolism are encountered in plants and frequently consist of tandem duplicated copies of one or more gene families (Nützmann et al., 2016, 2018). The molecular mechanisms driving the formation and evolution of

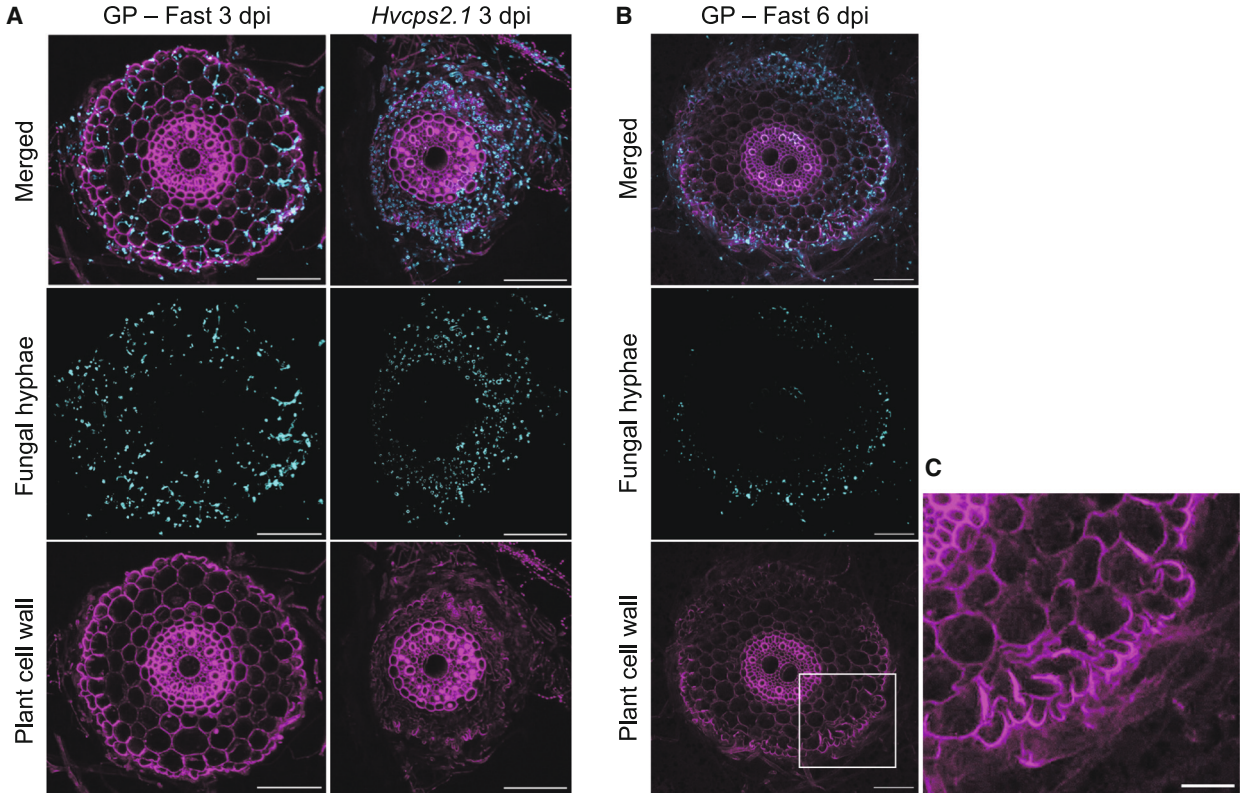

D

ENSEMBL GENE ID	Description	Differential expression over time						Differential expression on planta (Sarkar *et al.*, 2019)	
		24 hpi		48 hpi		72 hpi			
		Log2FC	p.adj	Log2FC	p.adj	Log2FC	p.adj	Log2FC	p.adj
COCSADRAFT_41732	glycoside hydrolase family 128 protein	-0.113	0.755	**0.418**	0.032	**1.836**	0.040	*NA*	*NA*
COCSADRAFT_173335	carbohydrate-binding module family 1 protein	0.211	0.815	**0.807**	0.000	**1.757**	0.000	**5.97**	2e-44
COCSADRAFT_170011	Isochorismatase hydrolase-like protein	0.254	0.828	0.695	0.272	**1.617**	0.004	**1.69**	0.056
COCSADRAFT_222726	glycoside hydrolase family 5 protein	-0.223	0.742	0.503	0.080	**1.387**	0.016	**4.33**	2e-11
COCSADRAFT_113651	FAD-binding domain-containing protein	**0.455**	0.010	**0.660**	0.000	**1.189**	0.000	**1.63**	4e-04
COCSADRAFT_137205	Peroxidase	0.182	0.613	**-0.586**	0.004	**-1.470**	0.004	**0.74**	0.048
COCSADRAFT_184162	FAD-binding domain-containing protein	**0.919**	0.000	**-0.443**	0.032	**-1.661**	0.000	**1.68**	0.014
COCSADRAFT_285519	lytic polysaccharide monooxygenase	0.042	0.923	**-0.668**	0.000	**-1.821**	0.008	**-1.24**	9e-04
COCSADRAFT_40808	glycoside hydrolase family 5 protein	*NA*	*NA*	0.417	0.674	**-2.500**	0.043	**-1.29**	1e-03
COCSADRAFT_38316	endonuclease/exonuclease/phosphatase family protein-like protein	-0.237	0.541	-0.338	0.302	**-2.930**	0.000	**2.67**	6e-19
COCSADRAFT_202450	CYP60b like	**6.871**	0.000	**7.621**	0.000	**4.453**	0.000	**-1.54**	0.383
COCSADRAFT_46028	Cytochrome P450	**5.672**	0.000	**8.645**	0.000	**2.873**	0.000	*NA*	*NA*
COCSADRAFT_197249	CYP60b like	**1.881**	0.000	**2.914**	0.000	**2.532**	0.000	*NA*	*NA*
COCSADRAFT_183275	MFS-type transporter	**5.213**	0.000	**6.138**	0.000	**4.456**	0.000	**7.36**	3e-55
COCSADRAFT_198203	MFS-type transporter	0.309	0.129	**0.975**	0.000	**2.546**	0.003	*NA*	*NA*

Figure 7. Microscopic observation of WT and *Hvcps2* roots colonized by *Bs* at 3 and 6 dpi.
(A) Cross-sections of WT (GP-Fast) and *Hvcps2.1* barley roots infected by *Bs* at 3 dpi. In *Hvcps2.1* mutants the outer cell layers, epidermis and sub-epidermis, are extensively damaged, indicating necrotrophy.
(B) Cross-section of WT (GP-Fast) barley roots infected by *Bs* at 6 dpi.

(legend continued on next page)

these clusters are still enigmatic, but the physical association and duplication of genes offer a number of potential advantages. First, physical association means that possible toxic intermediates due to mutation or loss of one of the genes are less likely to accumulate. Second, the presence of multiple copies of highly similar genes provides opportunities for gene rearrangements and independent evolution, thereby opening the door to rapid chemical innovations. The capacity to evolve novel defenses rapidly constitutes a key evolutionary adaptation in the arms race against pests and pathogens. The chromosome 2 barley biosynthetic gene cluster (BGC), which is related to the rice momilactone BGC, is conserved throughout the grasses, and Wu et al. (2022), through an extensive analysis of genome sequences, proposed that the rice BGC evolved from a Triticeae cluster via lateral gene transfer. How this lateral gene transfer occurred, however, remains highly speculative.

Barley diterpenoid phytoalexins show distinct effects on different pathogenic fungi

Thanks to the reconstitution of the barley diterpenoid biosynthesis in yeast, we could purify one of the most highly functionally decorated diterpenoids, 19-OH-HTA, and quantify it accurately using NMR. This allowed us to estimate its concentration in the medium surrounding the root upon elicitation at around 1 μM (Supplemental Figure 22), which is in the same range as the concentration of momilactones found in root medium (0.21–1.45 μM and 0.66–3.84 μM for momilactone A and B, respectively [Kato-Noguchi et al., 2010]). Notably, we found that 19-OH-HTA had contrasting effects on different fungi, being highly antifungal against *Fg* and *Sv* while stimulating the growth of *Bs* (Figure 4) at concentrations that are in the same range as those found in root exudates. Confirming these results, the colonization of barley *Hvcps2* mutants unable to produce diterpenoids by *Fg* was increased by almost 4 -fold, while it was reduced for *Bs* (Figure 5). Further in favor of the positive role of the barley diterpenoids in supporting colonization of roots by *Bs*, colonization levels measured by RT–qPCR were restored when extracts containing 19-OH-HTA were supplied to *Hvcps2* mutants. Collectively, these results show that barley hordedanes have strong antifungal activity and largely contribute to restricting the fungal growth of *Fg*, but that *Bs* has adapted to these diterpenoids.

A delayed necrotrophic phase induced by barley diterpenoids

A broadly reported mechanism by which microbial pathogens circumvent the toxicity of phytoalexins is via enzymatic degradation or modification (Westrick et al., 2021). Much less frequent is the modification of phytoalexins to modulate plant–pathogen interactions. To our knowledge, the only documented example is that of α-tomatine, a steroidal glycoalkaloid from tomato, which is partially deglycosylated to β_2-tomatine by tomatinase from the fungal pathogen *Septoria lycopersici* (Osbourn et al., 1995). In addition to detoxifying α-tomatine, tomatinase and β_2-tomatine suppress plant defense (Bouarab et al., 2002). This, however, was shown in a heterologous host, *N. benthamiana*, and the mechanism by which β_2-tomatine and tomatinase repress plant defenses is still unknown. Here, it was found that *Bs* can oxidize 19-OH-HTA and conjugate it to its own sesquiterpenoids (Figure 6 and Supplemental Data 1, **37** and **38**). Transcriptomics data revealed a significant reprogramming with a total of 307 genes that are differentially expressed in at least one of the three time points (Supplemental Data 2). Importantly, we found potential candidates for the oxidation of barley diterpenoids, such as CYPs and transporters, as well as genes involved in pathogenicity such as glycoside hydrolases or isochorismatase, both of which are predicted to be secreted (Figure 7D, Supplemental Data 2). Glycoside hydrolases play a role in degrading the plant cell wall and are likely required to facilitate the penetration of the fungus inside the roots, while isochorismatase was found to be secreted by two plant pathogenic microorganisms (*Phytophthora infestans* and *Vd*) to disrupt the biosynthesis of salicylic acid, which is a well-established defense hormone (Liu et al., 2014). Additionally, we found several downregulated genes encoding secreted proteins that have been suggested to play a role in the transition to the necrotrophic phase. These include an exonuclease/endonuclease/phosphatase family protein (COCSADRAFT-38316) and an LPMO (COCSADRAFT_285519). Interestingly, a DNA nuclease was found to be involved in triggering cell death by *Sv* (Dunken et al., 2022). Furthermore, LPMOs have been associated with the switch to the necrotrophic phase of hemibiotrophic fungi (Valente et al., 2011; O'Connell et al., 2012; Yakovlev et al., 2012). Previous transcriptome data produced from root inoculation of barley by *Bs* gave similar expression changes for the genes mentioned above (Figure 7D). This validates the transcriptional changes observed in axenic cultures of *Bs* treated with 19-OH-HTA. Microscopy observations at 3 and 6 dpi of WT and *Hvcps2* mutants showed that *Hvcps2* mutants at 3 dpi already displayed extensive damage of the outer cell layers of the root, which only occurred at 6 dpi in the WT (Figure 7A–7C). This fits with the downregulation of genes by 19-OH-HTA that could contribute to cell death (exo-endonuclease and LPMO). A premature switch to the necrotrophic phase could lead to a reduced progression of the fungus. This provides clues toward further understanding the interaction between *Bs* and barley. This could be done, for example, by mutating some of the *Bs* candidate genes identified via the transcriptomics approach using CRISPR/Cas9-mediated gene editing and investigating the infection phenotype of these mutants on WT and *Hvcps2* mutants.

In conclusion, our study elucidates the biosynthesis of some of the major barley diterpenoid phytoalexins. Through a combination of metabolic engineering, molecular genetics, infection assays, transcriptomics, and cell biology, we uncover how *Bs* circumvents the metabolic defense of barley and even exploits it to facilitate root colonization. Considering that diterpenoids are only one group of compounds produced in response to

(C) Detail of altered WT (GP-Fast) root structure from region designated by a white square in **(B)**. Magenta: plant cell wall stained with 10 μg ml^{-1} propidium iodide; cyan: fungal cell wall stained with 0.5 μg ml^{-1} WGA-AlexaFluor488. Scale bars in **(A)–(C)**, 100 μm.

(D) Table showing a selection of *Bs* genes differentially regulated by 19-OH-HTA with relevance to pathogenicity. Given are the gene IDs from the ENSMBL database, the description of the gene based on BLAST searches, the $\log_2$ fold change (treatment with 19-OH-HTA versus no treatment) at 24, 48, and 72 h, and $\log_2$ fold change of *Bs* genes compared to *Bs* in axenic culture during *in planta* infection of barley roots from Sarkar et al. (2019).

pathogens, our work illustrates the complexity of interactions at the metabolite level between pathogens and plant hosts. Deciphering these specific interactions will allow us to better understand plant defense mechanisms besides the classical gene-for-gene resistance.

METHODS

Plant growth and fungal inoculations

Barley seeds (*Hordeum vulgare* L. cv. Golden Promise) were sterilized in 70% ethanol for 1 min, followed by washing with sterile distilled water and 1.5-h incubation in 12% sodium hypochloride under continuous shaking. After 30-min washing three times, the seeds were placed on wet filter paper in darkness and at room temperature for 4 days for germination. Four seedlings were transferred to 1/10 PNM (plant nutrition medium, pH 5.7) (Wawra et al., 2016) in sterile glass jars (height 147 mm, mouth 100 mm; WECK) and grown in a day/night cycle of 16/8 h at 22°C/18°C, 60% humidity under 108 μmol m^{-2} s^{-1} light intensity.

Bipolaris sorokiniana (ND90Pr, *Bs*) was used in this study. *Bs* was propagated on modified CM medium (36) with 1.5% agar in darkness at 28°C for 21 days before inoculation. *Bs* conidia were collected according to the procedures described in Sarkar et al. (2019). Barley roots were inoculated with 5 ml of *Bs* conidia (5000 spores ml^{-1}) per jar for 6 days. Sterile water was used as a mock treatment. Roots were washed thoroughly, and the corresponding media were collected and snap-frozen in liquid nitrogen for extraction of metabolites.

Phylogenetic analysis

Phylogenetic analysis was conducted using MEGA X (Kumar et al., 2018b). Protein sequences (Supplemental Tables 2–4) were first aligned using the ClustalW algorithm (Thompson et al., 1994), after which phylogenetic trees were generated from the alignment using the maximum-likelihood method with a bootstrap of 1000. For the other parameters, default settings were used.

RT–qPCR

RNA isolation from roots was performed using the Spectrum Plant Total RNA kit (Sigma-Aldrich). Complementary DNA (cDNA) was synthesized using the ProtoScript II First Strand cDNA Synthesis Kit (New England Biolabs) following the manufacturer's instructions with primer $d(T)_{23}$ VN. Real-time qPCR was performed in triplicates using 10–20 ng of cDNA as template and gene specific primer pairs shown in Supplemental Table 11 in a CFX Connect Real-Time PCR System (Bio-Rad). The PCR conditions were 95°C for 15 min; 40 cycles of 95°C for 15 s, 60°C for 30 s; 95°C for 10 s. The melting curve was measured from 65°C to 95°C with a step of 0.1°C per second. Relative expression of targeted genes was calculated using delta Ct method (Livak and Schmittgen, 2001) and the barley ubiquitin gene as reference (Deshmukh et al., 2006).

Heterologous expression of diterpenoid biosynthesis genes in yeast

Plasmids containing *GGPPS* and *ATR1* were kindly provided by colleagues in the group and have been described previously (Scheler et al., 2016). Codon-optimized DNA sequences of *HvCPS2*, *HvKSL4*, *HvCYP89E31*, *HvCYP99A66*, *HvCYP99A67*, and *HvCYP99A68* were synthesized by Thermo Fisher Scientific for yeast expression. Each gene was further cloned into Golden Gate compatible yeast expression level 1 vector, together with a synthetic galactose-inducible promoter and a terminator. Different gene combinations were finally assembled into one yeast expression level M vector by a 50-cycle restriction–ligation reaction with *Bpi*I and T4-ligase.

Constructs were then transformed into *Saccharomyces cerevisiae* strain INVSc1 (Thermo Fisher Scientific) and plated out onto uracil-free (Ura^-) selection medium (1 g l^{-1} yeast synthetic drop-out medium supplements without uracil [Sigma-Aldrich], 6.7 g l^{-1} yeast nitrogen base with amino acids [Sigma-Aldrich]. and 20 g l^{-1} micro agar [Duchefa Biochemie]). Three positive colonies were picked and inoculated into 5 ml of yeast extract-peptone-dextrose (YPD) medium (20 g l^{-1} tryptone and 10 g l^{-1} yeast extract) containing 2% of glucose and grown for 24 h with shaking at 30°C. To induce protein expression, the cell pellet was resuspended in fresh YPD medium containing 2% galactose. After another 24 h of growth, the whole culture was extracted with 2 ml of *n*-hexane.

Transient expression in *N. benthamiana*

Transit peptides of protein HvCPS2 and HvKSL4 were predicted by two online tools, ChloroP 1.1 (http://www.cbs.dtu.dk/services/ChloroP/) and LOCALIZER (http://localizer.csiro.au/). Truncated sequences without the predicted transit peptides of these two genes were generated by PCR reactions using designed primers (Supplemental Table 11) and subsequently sequenced. The cDNAs of truncated *HMG reductase* and *GGPPS* in plasmids have been described previously (Scheler et al., 2016; Yadav et al., 2019). The *trHMG reductase*, *GGPPS*, *trHvCPS2*, *trHvKSL4*, *HvCYP89E31*, *HvCYP99A66*, *HvCYP99A67*, and *HvCYP99A68* were cloned into T-DNA vectors (binary vector pL1F-1) driven by the 35S promoter and flanked by the Ocs terminator (Weber et al., 2011). The resulting T- DNA plasmids were transformed into *Agrobacterium tumefaciens* strain GV3101pMP90 and plated out onto LB agar plates with appropriate antibiotics. Bacteria were harvested and resuspended in infiltration medium (10 mM $MgCl_2$, 10 mM 2-(*N-morpholino)ethanesulfonic* acid, 20 μM acetosyringone, pH 5.6) after 48 h of inoculation at 28°C. To co-infiltrate several genes, each bacteria suspension was diluted to a final OD_{600} of 0.4, after which all strains were mixed equally to an appropriate volume for infiltration. The suspension was infiltrated into the abaxial side of several leaves in three individual 4-week-old *N. benthamiana* plants using a syringe without needle. After treatment, the plants were cultivated in a climate-controlled phytochamber for 4 days. Three leaf disks (9-mm diameter) per infiltrated spot were harvested and extracted by 2 ml of *n*-hexane, followed by drying down under nitrogen flow and GC/LC–MS analysis.

Microsome isolation and *in vitro* enzyme assay

A protocol from the literature with slight modification was used for microsome isolation (Urban et al., 1997; Scheler et al., 2016). The construct carrying *HvCYP89E31* and *ATR1* were transformed into yeast strain INVSc1. A single positive colony was picked to inoculate 5 ml of Ura^- medium with 2% glucose and grown for 24 h at 30°C with shaking. The culture was then used to inoculate 100 ml

of Ura$^-$ medium with 2% glucose in a 500-ml flask at 30°C for 24 h. The cells were collected by centrifugation, resuspended in 100 ml of fresh YPD medium with 2% galactose to induce protein expression, and inoculated under shaking for another 24 h at 30°C. All the following steps were carried out at 4°C. The cells were harvested by centrifugation and resuspended in 30 ml of pre-chilled TEK buffer (50 mM Tris–HCl [pH 7.5], 1 mM EDTA, 100 mM KCl), centrifuged again, and resuspended in 2 ml of TES buffer (50 mM Tris–HCl [pH 7.5], 600 mM sorbitol, 10 g l^{-1} BSA, 1.5 mM β-mercaptoethanol) and transferred to a 50-ml tube. Acid-washed autoclaved glass beads 450–600 μm in diameter were added into the tube until the surface of the cell suspension was reached. The suspension was shaken vigorously by hand for 1 min and returned to ice for 1 min. This step was repeated four times. The glass beads were washed by 5 ml of TES buffer three times, and the supernatant was collected and combined into a new tube, followed by centrifugation at 7500 *g* for 10 min. The supernatant was transferred to ultracentrifugation tubes and centrifuged for 2 h at 100 000 *g*. The pellet was gently washed successively with 5 ml of TES and 2.5 ml of TEG buffer (50 mM Tris–HCl [pH 7.5], 1 mM EDTA, 30% glycerol) after the supernatant was removed, then transferred to a Potter homogenizer with a spatula. Two milliliters of TEG buffer was added to the homogenizer, and the pellet was carefully homogenized. Aliquots (100 μl) were transferred to 1.5-ml microtubes and stored at −80°C until used.

In vitro CYP enzyme assays were performed in a 600-μl reaction volume containing 40 μl of microsome preparation, 100 μM substrate, 1 mM NADPH, and 50 mM sodium phosphate (pH 7.4). The solution was incubated at 30°C for 2 h with gentle shaking. Products were extracted with 1 ml of *n*-hexane under strong agitation (vortex). After centrifugation, the organic phase was collected, then dried under a N_2 stream and resuspended in 100 μl of *n*-hexane for GC–MS analysis.

Purification of diterpenoids from yeast culture by silica gel column chromatography or SPE

For the purification of hordediene (**1**), 1 l of yeast culture was grown and extracted with 1 l of *n*-hexane. The raw extracts were dried in a rotary evaporator and resuspended in 4 ml of *n*-hexane, then loaded into two properly conditioned SiOH solid-phase extraction (SPE) cartridges (500 mg, Macherey-Nagel, Düren, Germany). The cartridges were then washed with 2 ml of *n*-hexane. The breakthrough and washing fractions were collected and combined. After drying down under nitrogen stream, an aliquot was measured by GC–MS to check the purity of the product and the rest, with an amount of around 2 mg being used for NMR structure elucidation.

Diterpenoids **5**, **6**, and **8** were first extracted from 3 l of yeast culture. After concentration, the raw extracts were dissolved in 4 ml of *n*-hexane and loaded into a pre-conditioned self-packed silica gel column (5 g, 15 mm × 100 mm). The column was then eluted by *n*-hexane and successively by 99:1, 98:2, 97:3, 96:4, and 95:5 *n*-hexane:ethyl acetate solutions. The volume of every elution solution was 10 ml, and each elution was sequentially collected into five 2-ml microtubes. An aliquot of each fraction was measured by GC–MS, and the fractions with the same product were combined and then used for NMR structure elucidation. The yields of diterpenoids **5** and **8** were around 0.5 mg, and that of **6** was about 1 mg.

Diterpenoids **19** and **21** were first extracted from 3–5 l of yeast culture by the same volume of extraction solution (95:5 *n*-hexane:ethyl acetate). After concentration, the raw extracts were dissolved in 4 ml of *n*-hexane and loaded into two properly conditioned SiOH SPE cartridges (500 mg, Macherey-Nagel). The column was then washed by 2 ml of *n*-hexane and successively by 2 ml of 95:5, 90:10, and 85:15 *n*-hexane:ethyl acetate solutions, followed by elution using 80:20 *n*-hexane/ethyl acetate for **19** or 75:25 *n*-hexane:ethyl acetate for **21**. The volume of elution solution was 10 ml, but the elution was separately collected into five 2-ml microtubes. An aliquot of each fraction was measured by LC–MS, and the fractions with the same product were combined and then used for NMR structure elucidation. The yields of diterpenoids **19** and **21** were around 1 mg and 0.5 mg, respectively.

Purification of diterpenoid 35 from barley root exudates

Purification of semi-polar diterpenes was achieved by micro-SPE-ultraperformance liquid chromatography (UPLC)–MS on a prototype device (Axel Semrau, Sprockhövel, Germany). In brief, 400 μl of methanolic barley or yeast extracts (dissolved in 80% methanol acidified to pH 2.4) were injected to micro-SPE cartridges (CHROspe Polymer DVB 10 × 2 mm, 25–35 μM, SparkHolland, Emmen, the Netherlands) under concomitant dilution by a second pump with an excess of water. Next, adsorbed diterpenoids were transferred from the SPE cartridge to a UPLC column (Nucleoshell RP18, 2 mm × 100 mm × 2.7 μm) with 400 μl of 80% acetonitrile used for desorption. During the transfer, the eluate was diluted with water again to give a final concentration of 8% acetonitrile on column throughout the transfer process. Barley and yeast-derived diterpenoids were chromatographically separated using the gradient described above, but fractions were collected from the UPLC effluent. Micro-SPE was again used for fraction collection, and the LC effluent was again diluted with excess water to retain the desired products. Finally, the SPE cartridges were desorbed with pure methanol and the eluates dried in a nitrogen stream.

NMR conditions

^{1}H, ^{13}C, ^{2}D (^{1}H,^{1}H gDQCOSY; ^{1}H,^{1}H zTOCSY;^{1}H,^{1}H ROESYAD; ^{1}H,^{13}C gHSQCAD;^{1}H,^{13}C gHMBCAD), selective (^{1}H,^{1}H zTOCSY1D; ^{1}H,^{1}H ROESY1D), and band-selective (^{1}H,^{13}C bsHMBC) NMR spectra were measured with an Agilent VNMRS 600 instrument at 599.83 MHz (^{1}H) and 150.84 MHz (^{13}C) using standard CHEMPACK 8.1 pulse sequences implemented in the VNMRJ 4.2A spectrometer software. TOCSY mixing time: 80 ms; ROESY mixing time: 300 ms; HSQC optimized for ^{1}JCH = 146 Hz; HMBC optimized for ^{n}JCH = 8 Hz. All spectra were obtained with C_6D_6 + 0.03% TMS as solvent at +25°C. Chemical shifts were referenced to internal TMS (δ ^{1}H = 0 ppm) and internal C_6D_6 (δ ^{13}C = 128.0 ppm). Quantitative ^{1}H NMR was performed with hexamethyldisiloxane as internal standard with 90° pulse width (pw = 6.8 μs), 17.27 s relaxation time, and 2.73 s acquisition time.

Metabolite extraction from barley roots and PNM medium

One hundred milligrams (fresh weight) of frozen and cryo-ground root matter was extracted using 900 μl of dichloromethane/ethanol

(2:1, v/v) and 100 μl of hydrochloric acid solution (pH 1.4). Extraction and duplicate removal of hydrophilic metabolites was achieved by 1-min FastPrep bead milling (FastPrep24, MP Biomedicals) followed by phase separation during centrifugation. For extraction, 1.6 ml of wall-reinforced cryo-tubes (Biozyme) each containing steel and glass beads were used. The upper aqueous phase was discarded and replaced for a second round of bead mill extraction/centrifugation. Thereafter, the aqueous phase was removed, and the lower organic phase was collected. Subsequently 600 μl of tetrahydrofuran (THF) was used for exhaustive extraction (FastPrep). After centrifugation, the organic THF extract was combined with the first extract and dried under a stream of N_2.

Root exudates were extracted from 60 ml of Gelrite medium. For this, the gel was distributed into two 50-ml Falcon tubes. To each tube, 4 ml of ethyl acetate was added. The tubes were thoroughly shaken by hand and centrifuged. The upper phase (organic extract) was collected before fresh ethyl acetate was added for another two consecutive extractions. The combined extracts of three extraction rounds were combined and dried in a stream of N_2.

GC–MS

Dried extracts were suspended in 200 μl of *n*-hexane. Analysis of yeast and plant extracts was carried out using a Trace GC Ultra gas chromatograph (Thermo Scientific) coupled to an ATAS Optic 3 injector and an ISQ single-quadrupole mass spectrometer (Thermo Scientific) with electron impact ionization. Chromatographic separation was performed on a ZB-5MS capillary column (30 m × 0.25 mm × 0.25 mm, Phenomenex) using splitless injection and an injection volume of 1 μl. The injection temperature rose from 60°C to 250°C at 7°C s^{-1} and the flow rate of helium was 2 ml min^{-1}. The GC oven temperature ramp was as follows: 50°C for 1 min, 50°C–300°C at 7°C min^{-1}, 300°C–330°C at 20°C min^{-1}, and 330°C for 5 min. Mass spectrometry was performed at 70 eV, in a full scan mode with *m/z* from 50 to 450. Data analysis was conducted using the device-specific software Xcalibur (Thermo Scientific).

Some samples were analyzed on a ZB-5HT capillary column (30 m × 0.25 mm × 0.25 mm, Phenomenex) using splitless injection and an injection volume of 1 μl. The injection temperature rose from 130°C to 280°C at 5°C s^{-1}, and the flow rate of helium was 2 ml min^{-1}. The GC oven temperature ramp was as follows: 130°C for 2 min, 130°C–250°C at 8°C min^{-1}, 250°C–310°C at 10°C min^{-1}, and 310°C for 5 min. MS spectra were acquired using the same parameters described above.

Reverse-phase UPLC–MS/MS and ESI–MS/MS

For UPLC–MS/MS analysis, dried extracts were suspended in 180 μl of 80% methanol/20% water. Separation of medium polar metabolites was performed on a Nucleoshell RP18 (2.1 × 150 mm, particle size 2.1 μm, Macherey-Nagel) using a Waters ACQUITY UPLC System, equipped with a binary solvent manager and sample manager (20-μl sample loop, partial loop injection mode, 5-μl injection volume; Waters, Eschborn, Germany). Eluents A and B were aqueous 0.3 mmol l^{-1} NH_4HCOO (adjusted to pH 3.5 with formic acid) and acetonitrile, respectively. Elution was performed isocratically for 2 min at 5% eluent B, from 2 to 19 min with a linear gradient to 95% B, from 19 to 21 min isocratically at 95% B, and from 21.01 to 24 min at 5% B. The flow rate was set to 400 μl min^{-1}, and the column temperature was maintained at 40°C. Metabolites were detected by positive and negative ESI and MS.

MS analysis of small molecules was performed by MS-time-of-flight (TOF)-SWATH–MS/MS (TripleToF 5600; AB Sciex, Darmstadt, Germany) operating in negative or positive ion mode and controlled by Analyst 1.7.1 software (AB Sciex). The source operation parameters were as follows: ion spray voltage, −4500 V/+5500 V; nebulizing gas, 60 psi; source temperature 600°C; drying gas, 70 psi; curtain gas, 35 psi.

TripleToF instrument tuning and internal mass calibration were performed every five samples with the calibrant delivery system applying APCI negative or positive tuning solution (AB Sciex), respectively.

TripleToF data acquisition was performed in MS^1-ToF mode and MS^2-SWATH mode. For MS^1 measurements, ToF masses were scanned between 65 and 1250 Da with an accumulation time of 50 ms and a collision energy of 10 V (−10 V). MS^2-SWATH experiments were divided into 26-Da segments of 20 ms accumulation time. Together, the SWATH experiments covered the entire mass range from 65 to 1250 Da in 48 separate scan experiments, which allowed a cycle time of 1.1 s. Throughout all MS/MS scans, a declustering potential of 35 V (or −35 V) was applied. Collision energies for all SWATH–MS/MS were set to 35 V (−35 V) and a collision energy spread of ±25 V, maximum sensitivity scanning, and otherwise default settings.

For some samples, MS analysis of small molecules was performed by MS-TOF-IDA–MS/MS (ZenoTOF 7600; AB Sciex) operating in negative or positive ion mode and controlled by SCIEX OS software 2.1.6 (AB Sciex). The source operation parameters were as follows: ion spray voltage, −4500 V/+5500 V; ion source gas 1, 60 psi; source temperature, 600°C; ion source gas 2, 70 psi; curtain gas, 35 psi; CAD gas, 7. ZenoTOF instrument tuning and internal mass calibration were performed every five samples with the calibrant delivery system applying X500 ESI negative or positive calibration solution (AB Sciex), respectively. ZenoTOF data acquisition was performed in MS^1-ToF mode and MS^2-IDA mode. For MS^1 measurements, ToF masses were scanned between 65 and 1500 Da with an accumulation time of 100 ms and a collision energy of 10 V (−10 V). MS^2-IDA experiments were performed using the following parameters: ToF mass range 65–1500; declustering potential of 80 V (or −80 V) with a spread of 50; maximum candidate ions of 40 with an intensity threshold of 1000 cps; collision energy of 35 V (−35 V) with a spread of 25 V; Zeno threshold 20 000 cps; accumulation time of 20 ms. Total scan time of one cycle for both MS^1 and MS^2 was 1.166 s.

Mutation of *HvCPS2* and *HvKSL4* by CRISPR/Cas9-mediated gene editing

The CRISPOR web tool (Concordet and Haeussler, 2018) was used to design two sgRNAs for each gene, as follows (PAM sequence underlined):

HvCPS2_gRNA1: 5′-GAAGAGTAGGGTCGTTGGTATGG-3′

HvCPS2_gRNA2: 5′ -AAGTTAATCTCGAAGCCACATGG-3′

HvKSL4_gRNA1: 5′ -GGCTGGTGAGTCAAATTCACCGG-3′

HvKSL4_gRNA2: 5′ -TTAATGTGATAGTTCGCCATCGG-3′

Golden Gate cloning was used to load each pair of guide sequences from complementary oligonucleotides into shuttle vectors pMGE625 and pMGE627, which were then assembled into binary vector pMGE599 to create pMP222 (HvCPS2) and pMP223 (HvKSL4). Vectors and cloning protocols have been previously described (Kumar et al., 2018a) and were kindly provided by Johannes Stuttmann. Stable transformation of pMP222 and pMP223 in Golden Promise Fast was performed as described by Amanda et al. (2022).

Root staining and fluorescence measurements

After harvesting, the roots were gently washed in distilled water, cut into 1-cm pieces, and placed in 2-ml test tubes filled with 1.5 ml of 50% ethanol (EtOH) overnight at 4°C. After removing the EtOH, the root segments were incubated in 20% potassium hydroxide (KOH) for 10 min at 90°C. The KOH was then removed, and the samples were washed three times with distilled water. Thereafter, the roots were incubated in 0.1 M hydrochloric acid (HCl) for 1.5 h at room temperature and then again washed three times with distilled water. The roots were rinsed with PBS once and then incubated in PBS-WGA staining solution (WGA-AlexaFluor488 final concentration of 0.5 μg ml^{-1}) overnight, wrapped in aluminum foil, at 4°C. A counterstain of the root cells was carried out with 10 μg ml^{-1} propidium iodide (PI).

The fluorescence of each segment was measured in a TECAN device (Tecan Group, Switzerland) with the following parameters: excitation wavelength 485 nm; emission wavelength 535 nm; gain 40% calculated on a WT sample; mirror dichroic 510; 30 flashes; *z*-position defined on a WT sample; 15 × 15 reads per well with a 2500-μm border. Four root pieces per sample were analyzed for each run. Eight runs per sample were carried out, therefore a total of 32 segments per sample were analyzed. Two samples per genotype were analyzed. After measuring, the average of each run was computed and used for statistical analysis.

Root sectioning and staining

Once harvested and cleaned, the roots were cut into 1-cm pieces and kept in PBS. Shortly after, these segments were embedded in 1% low melting agar in PBS with the help of a 1-ml syringe with the tip cut off. The obtained cylinders were then sliced by hand with a razor blade and a similar syringe for support. Slices of approximately 1 mm were laid on a glass slide, taking care to keep the original order and orientation as in the root. The staining was performed with the same solutions of WGA-AlexaFluor 488 and PI by adding around 100 μl on top of the slices for 10 min and washing in between with PBS.

Bioassay with 19-OH-HTA (21a) on five fungi

Bs (ND90Pr) was grown on modified CM-Bs medium (Sarkar et al., 2019). *S. vermifera* (MAFF305830; *Sv*) was grown on MYP medium (Lahrmann et al., 2015). *S. indica* (DSM11827; *Si*) was grown on CM medium (Hilbert et al., 2012). *V. dahliae* (JR2; *Vd*) was grown on PDA medium. *F. graminearum* (NL19-100008; *Fg*) was grown on YPSs medium (Cooney and Emerson, 1964). *Vd* was grown at room temperature in darkness for 7 days. All other fungi were grown at 28°C for 3 weeks. Spores were harvested as described previously (Sarkar et al., 2019) and diluted to a final concentration of 250 000 spores ml^{-1} for *Bs*, 700 000 spores ml^{-1} for *Si*, 552 000 spores ml^{-1} for *Fg*, and 542 500 spores ml^{-1} for *Vd* in 1/2 TSB (Sigma-Aldrich; 15 g l^{-1}). *Sv* small mycelium fragments were harvested by adding water to the plate, removing the loose hyphae with a scalpel, and filtering the solution through Miracloth. The solution was centrifuged, the supernatant was discarded, and the pellet was dissolved in 1/2 TSB medium. Four hundred microliters of the fungal solutions was applied to each microscope chamber slide (VWR; Kat734-2050) and treated with either 1% DMSO as a control or 1% DMSO + 10 μM of the barley diterpenoid **21a**. Pictures were taken at different time points depending on the speed of spore germination (3 h post inoculation [hpi] for *Bs*; 9 hpi for *Vd*; 9 hpi for *Fc*; 12 hpi for *Si*; and 12 hpi for *Sv*). Spore germination rate and tube elongation/hyphal length were quantified using ImageJ (Schneider et al., 2012).

Bioassay with 21a (19-OH-HTA) on *Bs* (growth curve)

To measure the growth curve of *Bs* in different concentrations of 19-OH-HTA (**21a**), the following assay was performed. Microplate wells were filled with 200 μl of working solution with different concentration of **21a**. Each concentration was tested with 10 replicates. After pipetting, the plate was inoculated at 28°C in either an incubator or TECAN device (Tecan Group). The value of OD_{405} was measured by TECAN every 1 h for over 96 h.

Final concentration of **21a** (μM)	**21a** stock (500 μM in DMSO) (μl)	DMSO (μl)	CM medium (μl)	*Bs* spore suspension (3×10^5 ml^{-1}) (μl)
Blank	0	20	980	0
0	0	20	880	100
1	2	18	880	100
5	10	10	880	100
10	20	0	880	100

Ingredients of the working solution

Note: final concentrations of **21a** were 0, 1, 5, and 10 μM in CM medium with 2% DMSO.

Kinetic assay *Bs* with 19-OH-HTA over 72 h

Two milliliters of growth medium prepared as for the bioassay (cf. preceding section) but without agar were inoculated with 10 μM 19-OH-HTA and incubated at 28°C under mild continuous shaking. An aliquot of 200 μl was collected at 0, 6, 10, 24, 34, 48, and 72 h, and extracted three times with 500 μl of ethyl acetate. The three fractions were then combined and dried under gaseous nitrogen flow. Prior to injection in LC–MS, the samples were resuspended in 50 μl of pure methanol.

Complementation assay

Growth of yeast and purification

The complementation assay was performed with two separate yeast extracts produced by two strains with a different plasmid, namely pAGT1009 and pAGT9593. pAGT1009 is an empty vector, while pAGT9593 contains the genes required to produce the 19-OH-HTA. *S. cerevisiae* strain INVSc1 was transformed, and positive colonies were grown in uracil-free medium (1 g l^{-1} yeast synthetic drop-out medium supplements without uracil [Sigma-Aldrich], 6.7 g l^{-1} yeast nitrogen base with amino acids [Sigma-Aldrich]) containing 2% glucose over 2 days under shaking at 30°C. The inoculum was then transferred to fresh medium containing 2% galactose to induce protein expression and grown over 3 days under the same conditions. A total of 3 l of medium was used for each strain. The whole culture was centrifuged for 20 min at maximum speed and 4°C. The supernatant was then loaded to a pre-conditioned self-packed SPE cartridge (5 g CHROMABOND HLB, 30 μm, Macherey-Nagel). The cartridge was washed with 200 ml of 1% acetic acid, and an elution gradient was performed with increasing concentrations of methanol. All fractions were measured via LC–MS. The fractions containing the compound 19-OH-HTA were then combined and diluted with 1% acetic acid to adjust the concentration of methanol back to 30%. This was loaded again into a similar SPE cartridge and, after washing as before, the elution was carried out with five fractions of 100 ml each of 100% methanol. Only the first fraction, which contained the compound 19-OH-HTA, was kept and dried down in a rotary evaporator. For the strain with the empty vector, the samples were processed the same way and the same fractions collected.

Preparation of the glass tubes

Barley growth medium (25 ml) was poured into a sterile glass tube in a slanted position (height 200 mm, mouth 30 mm; Carl Roth). After solidification, 5 ml of fresh agar containing either DMSO, the yeast extract producing 19-OH-HTA at 10 μM (pAGT9593), the yeast extract control (pAGT1009), or nothing was poured on top of the barley medium to create a uniform layer of approximately 1 cm.

Preparation of the glass jars

Barley medium (60 ml) was poured into a sterile glass jar (height 147 mm, mouth 100 mm; WECK) where a small glass vial was sitting in the center. This was removed once the agar solidified, leaving behind a hole of around 5-ml volume in which fresh agar, enriched with the different extracts, was later poured. Before adding the extracts to the agar, they were resuspended in pure DMSO to a final concentration of 2% in the 5-ml agar plug.

Seed sterilization and plant growth

Barley (*H. vulgare* L.) seeds cv. Golden Promise Fast and from the mutant *Hvcps2.1* were sterilized with 6% hypochlorite under continuous shaking for 1 h, then washed three times with sterile distilled water and four times under continuous shaking for 30 min each round. The seeds were placed on wet filter paper and allowed to germinate in darkness at room temperature over 3 days. The seedlings were then moved to the tubes (one per jar), taking care to position the roots over the yeast extract plug, and allowed to grow for a further 2 days. Next, the roots were inoculated with 5 ml of *Bs* conidia (5000 spores ml^{-1}), collected as already described (cf. "plant growth and fungal inoculations"), and grown over 6 days in a day/night cycle of 16/8 h at 22°C/18°C, 60% humidity under 108 μmol m^{-2} s^{-1} light intensity. Sterile water was used as a mock treatment. Roots were washed thoroughly, and the corresponding media were collected and snap-frozen in liquid nitrogen for extraction of metabolites and RNA extraction.

RNA extraction, cDNA synthesis, and Bs quantification via qPCR

See the section "RT–qPCR."

Estimation of 19-OH-HTA concentration in root exudates

WT plants were treated and grown as per standard protocol (cf. "seed sterilization and plant growth") in triplicates in glass tubes (height 200 mm, mouth 30 mm; Carl Roth) instead of Mason jars. The agar from the glass tubes was harvested at 2, 4, and 6 days after infection and sliced with the help of a razor blade in an upper layer of approximately 1 cm and a lower layer with the remaining agar. These two fractions were extracted three times with 5 ml of ethyl acetate, which was then combined and dried under gaseous nitrogen flow. Once resuspended in pure methanol, the samples were measured via LC–MS, and the concentration of the compound 19-OH-HTA was estimated with the help of a calibration curve of a purified standard quantified by NMR.

Fusarium graminearum infection assay

The same setup used for *Bs* was also used for *F. graminearum infection assay.*

mRNA-seq on *Bs* treated with 19-OH-HTA

Bs spores were incubated with 10 μM 19-OH-HTA over the course of 3 days, and four replicates per treatment were harvested every 24 h. Each sample (biological replicate) is the result of three pooled samples combined during harvest. Once harvested, the samples were centrifuged for 10 min at 4°C and maximum speed in a table-top centrifuge. The supernatant was removed. The pellet was snap-frozen in liquid nitrogen and freeze-dried over the course of 4 h. Once dried, the samples were ground in a ball mill, and total RNA was extracted using Spectrum Plant Total RNA (Merck) following the manufacturer's instructions. Total RNA was sent to Novogene for library preparation via poly(A) enrichment, followed by sequencing (paired end 150 bp, 5 gigabytes of raw data per sample) on a NovaSeq X Plus Series (Illumina). The obtained raw reads were then fed to the nf-core/rnaseq (Ewels et al., 2020) pipeline with default parameters for analysis. Both reference genome and gene annotation files for *Bs* nd90pr were downloaded from the JCI Genome Portal (Nordberg et al., 2014). Data mining and differential expression analysis were performed on R Statistical Software (v4.3.3; R Core Team, 2024) using DESeq2 (Love et al., 2014).

Synteny analysis

Synteny analysis was performed by MCScanX (Wang et al., 2012b), employing the parameters "-s 5 -w 0 -m 15." The orthologs were identified by the blastp program using the parameters "E-value 1e-10; num of best hits 10." The plot for micro-synteny was generated by MCScan (Python version) (Tang et al., 2008). The version of genomes used for the

analysis is IRGSP-1.0 of rice, MorexV2 of barley, and IWGSC RefSeq v1.0 of wheat.

DATA AND CODE AVAILABILITY

All data and materials are available on request to the corresponding author. The RNA-seq data of *Bs* with or without 19-OH-HTA have been deposited in GenBank (NCBI) and are accessible under Bioproject PRJNA1131952 and sequence read archive SUB14584410.

SUPPLEMENTAL INFORMATION

Supplemental information is available at *Molecular Plant Online*.

FUNDING

This work was funded by grants TI 800/7-1 and TI 800/7-2 (SPP 2125 DECRyPT) from the Deutsche Forschungsgemeinschaft, Germany, to A.T. We also acknowledge support from the Cluster of Excellence on Plant Sciences (CEPLAS) funded by the Deutsche Forschungsgemeinschaft under Germany's Excellence Strategy-EXC 2048/1-Project ID: 390686111 and the grant ZU 263/11-2 (SPP 2125 DECRyPT) to A.Z.

AUTHOR CONTRIBUTIONS

Y.L. performed metabolite profiling, cloning, expression in yeast and *N. benthamiana*, purification of several diterpenoids, *Bs* growth assay, synteny analysis, metabolism of barley 19-OH-HTA by *Bs*, *Bs* infection assay, and screening of the mutants (*Hvcps2*, *Hvksl4*), and prepared figures and materials. D.E. performed *Bs* growth assays, fluorescence staining and quantification, complementation experiments 19-OH-HTA, kinetic assays of *Bs* treated with 19-OH-HTA, microscopy of infected roots, and production and analysis of *Bs* transcriptome data. and prepared figures and materials. L.K.M. prepared inoculated barley material and performed fungal growth assays. A.P., H.H., and P.S. performed NMR spectroscopy and analysis. A.S.-H. assisted with metabolite profiling experiments. U.B. supervised the yeast engineering experiments. S.I. performed diterpene purifications from barley exudates. I.F.A. produced the CRISPR knockout mutants. A.Z. provided materials and co-initiated the project. G.U.B. supervised the metabolite profiling, analyzed the LC–MS data, and performed compound purification. A.T. conceived and designed the project, acquired funding, and wrote the manuscript.

ACKNOWLEDGMENTS

We would like to thank the gardeners of the Institute of Plant Biochemistry (IPB) for caring for the barley plants in the IPB greenhouses, and Edelgard Wendeler for her technical support with barley transformations. No conflict of interest declared.

Received: September 29, 2023
Revised: June 14, 2024
Accepted: July 10, 2024
Published: July 14, 2024

REFERENCES

Ahuja, I., Kissen, R., and Bones, A.M. (2012). Phytoalexins in defense against pathogens. Trends Plant Sci. **17**:73–90. https://doi.org/10.1016/j.tplants.2011.11.002.

Akatsuka, T., Kodama, O., Kato, H., Kono, Y., and Takeuchi, S. (1983). 3-Hydroxy-7-oxo-sandaracopimaradiene (oryzalexin A), a new phytoalexin isolated from rice blast leaves. Agric. Biol. Chem. **47**:445–447. https://doi.org/10.1271/bbb1961.47.445.

Amanda, D., Frey, F.P., Neumann, U., Przybyl, M., Šimura, J., Zhang, Y., Chen, Z., Gallavotti, A., Fernie, A.R., Ljung, K., and Acosta, I.F. (2022). Auxin boosts energy generation pathways to fuel pollen maturation in barley. Curr. Biol. **32**:1798–1811.e8. https://doi.org/10.1016/j.cub.2022.02.073.

Beier, S., Himmelbach, A., Colmsee, C., Zhang, X.-Q., Barrero, R.A., Zhang, Q., Li, L., Bayer, M., Bolser, D., Taudien, S., et al. (2017). Construction of a map-based reference genome sequence for barley, Hordeum vulgare L. Sci. Data **4**:170044. https://doi.org/10.1038/sdata.2017.44.

Block, A.K., Vaughan, M.M., Schmelz, E.A., and Christensen, S.A. (2019). Biosynthesis and function of terpenoid defense compounds in maize (Zea mays). Planta **249**:21–30. https://doi.org/10.1007/s00425-018-2999-2.

Bouarab, K., Melton, R., Peart, J., Baulcombe, D., and Osbourn, A. (2002). A saponin-detoxifying enzyme mediates suppression of plant defences. Nature **418**:889–892. https://doi.org/10.1038/nature00950.

Bruckner, K., and Tissier, A. (2013). High-level diterpene production by transient expression in Nicotiana benthamiana. Plant Methods **9**:46. https://doi.org/10.1186/1746-4811-9-46.

Cartwright, D., Langcake, P., Pryce, R.J., Leworthy, D.P., and Ride, J.P. (1977). Chemical activation of host defence mechanisms as a basis for crop protection. Nature **267**:511–513. https://doi.org/10.1038/267511a0.

Cho, E.-M., Okada, A., Kenmoku, H., Otomo, K., Toyomasu, T., Mitsuhashi, W., Sassa, T., Yajima, A., Yabuta, G., Mori, K., et al. (2004). Molecular cloning and characterization of a cDNA encoding ent-cassa-12,15-diene synthase, a putative diterpenoid phytoalexin biosynthetic enzyme, from suspension-cultured rice cells treated with a chitin elicitor. Plant J. **37**:1–8. https://doi.org/10.1046/j.1365-313X.2003.01926.x.

Christensen, S.A., Sims, J., Vaughan, M.M., Hunter, C., Block, A., Willett, D., Alborn, H.T., Huffaker, A., and Schmelz, E.A. (2018). Commercial hybrids and mutant genotypes reveal complex protective roles for inducible terpenoid defenses in maize. J. Exp. Bot. **69**:1693–1705. https://doi.org/10.1093/jxb/erx495.

Concordet, J.-P., and Haeussler, M. (2018). CRISPOR: intuitive guide selection for CRISPR/Cas9 genome editing experiments and screens. Nucleic Acids Res. **46**:W242–W245. https://doi.org/10.1093/nar/gky354.

Cooney, D.G., and Emerson, R. (1964). Thermophilic Fungi. (WH Freeman San Francisco).

De La Peña, R., and Sattely, E.S. (2021). Rerouting plant terpene biosynthesis enables momilactone pathway elucidation. Nat. Chem. Biol. **17**:205–212. https://doi.org/10.1038/s41589-020-00669-3.

Deshmukh, S., Hückelhoven, R., Schäfer, P., Imani, J., Sharma, M., Weiss, M., Waller, F., and Kogel, K.H. (2006). The root endophytic fungus Piriformospora indica requires host cell death for proliferation during mutualistic symbiosis with barley. Proc. Natl. Acad. Sci. USA **103**:18450–18457. https://doi.org/10.1073/pnas.0605697103.

Desmedt, W., Kudjordjie, E.N., Chavan, S.N., Zhang, J., Li, R., Yang, B., Nicolaisen, M., Mori, M., Peters, R.J., Vanholme, B., et al. (2022). Rice diterpenoid phytoalexins are involved in defence against parasitic nematodes and shape rhizosphere nematode communities. New Phytol. **235**:1231–1245. https://doi.org/10.1111/nph.18152.

Ding, Y., Murphy, K.M., Poretsky, E., Mafu, S., Yang, B., Char, S.N., Christensen, S.A., Saldivar, E., Wu, M., Wang, Q., et al. (2019). Multiple genes recruited from hormone pathways partition maize diterpenoid defences. Nat. Plants **5**:1043–1056. https://doi.org/10.1038/s41477-019-0509-6.

Ding, Y., Weckwerth, P.R., Poretsky, E., Murphy, K.M., Sims, J., Saldivar, E., Christensen, S.A., Char, S.N., Yang, B., Tong, A.D., et al. (2020). Genetic elucidation of interconnected antibiotic pathways mediating maize innate immunity. Nat. Plants **6**:1375–1388. https://doi.org/10.1038/s41477-020-00787-9.

Dunken, N., Widmer, H., Balcke, G.U., Straube, H., Langen, G., Charura, N.M., Saake, P., Leson, L., Rövenich, H., Wawra, S.,

et al. (2022). A fungal endophyte-generated nucleoside signal regulates host cell death and promotes root colonization. Preprint at bioRxiv. https://doi.org/10.1101/2022.03.11.483938.

Ewels, P.A., Peltzer, A., Fillinger, S., Patel, H., Alneberg, J., Wilm, A., Garcia, M.U., Di Tommaso, P., and Nahnsen, S. (2020). The nf-core framework for community-curated bioinformatics pipelines. Nat. Biotechnol. **38**:276–278. https://doi.org/10.1038/s41587-020-0439-x.

Fu, J., Ren, F., Lu, X., Mao, H., Xu, M., Degenhardt, J., Peters, R.J., and Wang, Q. (2016). A Tandem Array of ent-Kaurene Synthases in Maize with Roles in Gibberellin and More Specialized Metabolism. Plant Physiol. **170**:742–751. https://doi.org/10.1104/pp.15.01727.

Ghazvini, H., and Tekauz, A. (2008). Host-Pathogen Interactions Among Barley Genotypes and Bipolaris sorokiniana Isolates. Plant Dis. **92**:225–233. https://doi.org/10.1094/pdis-92-2-0225.

Gol, L., Haraldsson, E.B., and von Korff, M. (2021). Ppd-H1 integrates drought stress signals to control spike development and flowering time in barley. J. Exp. Bot. **72**:122–136. https://doi.org/10.1093/jxb/eraa261.

Harris, L.J., Saparno, A., Johnston, A., Prisic, S., Xu, M., Allard, S., Kathiresan, A., Ouellet, T., and Peters, R.J. (2005). The maize An2 gene is induced by Fusarium attack and encodes an ent-copalyl diphosphate synthase. Plant Mol. Biol. **59**:881–894. https://doi.org/10.1007/s11103-005-1674-8.

Hilbert, M., Voll, L.M., Ding, Y., Hofmann, J., Sharma, M., and Zuccaro, A. (2012). Indole derivative production by the root endophyte Piriformospora indica is not required for growth promotion but for biotrophic colonization of barley roots. New Phytol. **196**:520–534. https://doi.org/10.1111/j.1469-8137.2012.04275.x.

Huffaker, A., Kaplan, F., Vaughan, M.M., Dafoe, N.J., Ni, X., Rocca, J.R., Alborn, H.T., Teal, P.E., and Schmelz, E.A. (2011). Novel acidic sesquiterpenoids constitute a dominant class of pathogen-induced phytoalexins in maize. Plant Physiol. **156**:2082–2097. https://doi.org/10.1104/pp.111.179457.

Inoue, Y., Sakai, M., Yao, Q., Tanimoto, Y., Toshima, H., and Hasegawa, M. (2013). Identification of a Novel Casbane-Type Diterpene Phytoalexin, *ent*-10-Oxodepressin, from Rice Leaves. Biosci. Biotechnol. Biochem. **77**:760–765. https://doi.org/10.1271/bbb.120891.

Ishihara, A., Kumeda, R., Hayashi, N., Yagi, Y., Sakaguchi, N., Kokubo, Y., Ube, N., Tebayashi, S.-i., and Ueno, K. (2017). Induced accumulation of tyramine, serotonin, and related amines in response to Bipolaris sorokiniana infection in barley. Biosci. Biotechnol. Biochem. **81**:1090–1098. https://doi.org/10.1080/09168451.2017.1290520.

Jagadeeswaran, G., Veale, L., and Mort, A.J. (2021). Do Lytic Polysaccharide Monooxygenases Aid in Plant Pathogenesis and Herbivory? Trends Plant Sci. **26**:142–155. https://doi.org/10.1016/j.tplants.2020.09.013.

Jones, J.D., and Dangl, J.L. (2006). The plant immune system. Nature **444**:323–329. https://doi.org/10.1038/nature05286.

Jones, J.D.G., Staskawicz, B.J., and Dangl, J.L. (2024). The plant immune system: From discovery to deployment. Cell **187**:2095–2116. https://doi.org/10.1016/j.cell.2024.03.045.

Karunanithi, P.S., Berrios, D.I., Wang, S., Davis, J., Shen, T., Fiehn, O., Maloof, J.N., and Zerbe, P. (2020). The foxtail millet (Setaria italica) terpene synthase gene family. Plant J. **103**:781–800. https://doi.org/10.1111/tpj.14771.

Kato-Noguchi, H., and Ino, T. (2003). Rice seedlings release momilactone B into the environment. Phytochemistry **63**:551–554. https://doi.org/10.1016/S0031-9422(03)00194-8.

Kato-Noguchi, H., Ino, T., Sata, N., and Yamamura, S. (2002). Isolation and identification of a potent allelopathic substance in rice root exudates. Physiol. Plant. **115**:401–405. https://doi.org/10.1034/j.1399-3054.2002.1150310.x.

Kato-Noguchi, H., Hasegawa, M., Ino, T., Ota, K., and Kujime, H. (2010). Contribution of momilactone A and B to rice allelopathy. J. Plant Physiol. **167**:787–791. https://doi.org/10.1016/j.jplph.2010.01.014.

Kato, H., Kodama, O., and Akatsuka, T. (1993). Oryzalexin E, A diterpene phytoalexin from UV-irradiated rice leaves. Phytochemistry **33**:79–81. https://doi.org/10.1016/0031-9422(93)85399-C.

Kato, H., Kodama, O., and Akatsuka, T. (1994). Oryzalexin F, a diterpene phytoalexin from UV-irradiated rice leaves. Phytochemistry **36**:299–301. https://doi.org/10.1016/S0031-9422(00)97064-X.

Kato, T., Kabuto, C., Sasaki, N., Tsunagawa, M., Aizawa, H., Fujita, K., Kato, Y., Kitahara, Y., and Takahashi, N. (1973). Momilactones, growth inhibitors from rice, oryza sativa L. Tetrahedron Lett. **14**:3861–3864. https://doi.org/10.1016/S0040-4039(01)87058-1.

Kitaoka, N., Wu, Y., Xu, M., and Peters, R.J. (2015). Optimization of recombinant expression enables discovery of novel cytochrome P450 activity in rice diterpenoid biosynthesis. Appl. Microbiol. Biotechnol. **99**:7549–7558. https://doi.org/10.1007/s00253-015-6496-2.

Koga, J., Ogawa, N., Yamauchi, T., Kikuchi, M., Ogasawara, N., and Shimura, M. (1997). Functional moiety for the antifungal activity of phytocassane E, a diterpene phytoalexin from rice. Phytochemistry **44**:249–253. https://doi.org/10.1016/S0031-9422(96)00534-1.

Kono, Y., Takeuchi, S., Kodama, O., and Akatsuka, T. (1984). Absolute Configuration of Oryzalexin A and Structures of Its Related Phytoalexins Isolated from Rice Blast Leaves Infected with Pyricularia oryzae. Agric. Biol. Chem. **48**:253–255. https://doi.org/10.1271/bbb1961.48.253.

Kono, Y., Uzawa, J., Kobayashi, K., Suzuki, Y., Uramoto, M., Sakurai, A., Watanabe, M., Teraoka, T., Hosokawa, D., Watanabe, M., and Kondo, H. (1991). Structures of Oryzalides A and B, and Oryzalic Acid A, a Group of Novel Antimicrobial Diterpenes, Isolated from Healthy Leaves of a Bacterial Leaf Blight-resistant Cultivar of Rice Plant. Agric. Biol. Chem. **55**:803–811. https://doi.org/10.1080/00021369.1991.10870634.

Kumar, J., Schäfer, P., Hückelhoven, R., Langen, G., Baltruschat, H., Stein, E., Nagarajan, S., and Kogel, K.-H. (2002). Bipolaris sorokiniana, a cereal pathogen of global concern: cytological and molecular approaches towards better controldouble dagger. Mol. Plant Pathol. **3**:185–195. https://doi.org/10.1046/j.1364-3703.2002.00120.x.

Kumar, N., Galli, M., Ordon, J., Stuttmann, J., Kogel, K.H., and Imani, J. (2018a). Further analysis of barley MORC1 using a highly efficient RNA-guided Cas9 gene-editing system. Plant Biotechnol. J. **16**:1892–1903. https://doi.org/10.1111/pbi.12924.

Kumar, S., Stecher, G., Li, M., Knyaz, C., and Tamura, K. (2018b). MEGA X: Molecular Evolutionary Genetics Analysis across Computing Platforms. Mol. Biol. Evol. **35**:1547–1549. https://doi.org/10.1093/molbev/msy096.

Lahrmann, U., Strehmel, N., Langen, G., Frerigmann, H., Leson, L., Ding, Y., Scheel, D., Herklotz, S., Hilbert, M., and Zuccaro, A. (2015). Mutualistic root endophytism is not associated with the reduction of saprotrophic traits and requires a noncompromised plant innate immunity. New Phytol. **207**:841–857. https://doi.org/10.1111/nph.13411.

Li, Y.-Y., Tan, X.-M., Wang, Y.-D., Yang, J., Zhang, Y.-G., Sun, B.-D., Gong, T., Guo, L.-P., and Ding, G. (2020). Bioactive seco-Sativene Sesquiterpenoids from an Artemisia desertorum Endophytic Fungus, Cochliobolus sativus. J. Nat. Prod. **83**:1488–1494. https://doi.org/10.1021/acs.jnatprod.9b01148.

Liang, J., Merrill, A.T., Laconsay, C.J., Hou, A., Pu, Q., Dickschat, J.S., Tantillo, D.J., Wang, Q., and Peters, R.J. (2022). Deceptive Complexity in Formation of Cleistantha-8,12-diene. Org. Lett. **24**:2646–2649. https://doi.org/10.1021/acs.orglett.2c00680.

Liu, T., Song, T., Zhang, X., Yuan, H., Su, L., Li, W., Xu, J., Liu, S., Chen, L., Chen, T., et al. (2014). Unconventionally secreted effectors of two filamentous pathogens target plant salicylate biosynthesis. Nat. Commun. **5**:4686. https://doi.org/10.1038/ncomms5686.

Liu, Y., Balcke, G.U., Porzel, A., Mahdi, L., Scherr-Henning, A., Bathe, U., Zuccaro, A., and Tissier, A. (2021). A barley gene cluster for the biosynthesis of diterpenoid phytoalexins. Preprint at bioRxiv. https://doi.org/10.1101/2021.05.21.445084.

Livak, K.J., and Schmittgen, T.D. (2001). Analysis of Relative Gene Expression Data Using Real-Time Quantitative PCR and the $2^{-\Delta\Delta CT}$ Method. Methods **25**:402–408. https://doi.org/10.1006/meth.2001.1262.

Love, M.I., Huber, W., and Anders, S. (2014). Moderated estimation of fold change and dispersion for RNA-seq data with DESeq2. Genome Biol. **15**:550. https://doi.org/10.1186/s13059-014-0550-8.

Mascher, M., Wicker, T., Jenkins, J., Plott, C., Lux, T., Koh, C.S., Ens, J., Gundlach, H., Boston, L.B., Tulpová, Z., et al. (2021). Long-read sequence assembly: a technical evaluation in barley. Plant Cell **33**:1888–1906. https://doi.org/10.1093/plcell/koab077.

Miedaner, T., and Juroszek, P. (2021). Climate change will influence disease resistance breeding in wheat in Northwestern Europe. Theor. Appl. Genet. **134**:1771–1785. https://doi.org/10.1007/s00122-021-03807-0.

Miyazaki, S., Jiang, K., Kobayashi, M., Asami, T., and Nakajima, M. (2017). Helminthosporic acid functions as an agonist for gibberellin receptor. Biosci. Biotechnol. Biochem. **81**:2152–2159. https://doi.org/10.1080/09168451.2017.1381018.

Monat, C., Padmarasu, S., Lux, T., Wicker, T., Gundlach, H., Himmelbach, A., Ens, J., Li, C., Muehlbauer, G.J., Schulman, A.H., et al. (2019). TRITEX: chromosome-scale sequence assembly of Triticeae genomes with open-source tools. Genome Biol. **20**:284. https://doi.org/10.1186/s13059-019-1899-5.

Muchlinski, A., Jia, M., Tiedge, K., Fell, J.S., Pelot, K.A., Chew, L., Davisson, D., Chen, Y., Siegel, J., Lovell, J.T., and Zerbe, P. (2021). Cytochrome P450-catalyzed biosynthesis of furanoditerpenoids in the bioenergy crop switchgrass (Panicum virgatum L.). Plant J. **108**:1053–1068. https://doi.org/10.1111/tpj.15492.

Murphy, K.M., and Zerbe, P. (2020). Specialized diterpenoid metabolism in monocot crops: Biosynthesis and chemical diversity. Phytochemistry **172**:112289. https://doi.org/10.1016/j.phytochem.2020.112289.

Murphy, K.M., Edwards, J., Louie, K.B., Bowen, B.P., Sundaresan, V., Northen, T.R., and Zerbe, P. (2021). Bioactive diterpenoids impact the composition of the root-associated microbiome in maize (Zea mays). Sci. Rep. **11**:333. https://doi.org/10.1038/s41598-020-79320-z.

Nordberg, H., Cantor, M., Dusheyko, S., Hua, S., Poliakov, A., Shabalov, I., Smirnova, T., Grigoriev, I.V., and Dubchak, I. (2014). The genome portal of the Department of Energy Joint Genome Institute: 2014 updates. Nucleic Acids Res. **42**:D26–D31. https://doi.org/10.1093/nar/gkt1069.

Nürnberger, T., Nennstiel, D., Jabs, T., Sacks, W.R., Hahlbrock, K., and Scheel, D. (1994). High affinity binding of a fungal oligopeptide elicitor to parsley plasma membranes triggers multiple defense responses. Cell **78**:449–460. https://doi.org/10.1016/0092-8674(94)90423-5.

Nützmann, H.W., Huang, A., and Osbourn, A. (2016). Plant metabolic clusters - from genetics to genomics. New Phytol. **211**:771–789. https://doi.org/10.1111/nph.13981.

Nützmann, H.W., Scazzocchio, C., and Osbourn, A. (2018). Metabolic Gene Clusters in Eukaryotes. Annu. Rev. Genet. **52**:159–183. https://doi.org/10.1146/annurev-genet-120417-031237.

O'Connell, R.J., Thon, M.R., Hacquard, S., Amyotte, S.G., Kleemann, J., Torres, M.F., Damm, U., Buiate, E.A., Epstein, L., Alkan, N., et al. (2012). Lifestyle transitions in plant pathogenic Colletotrichum fungi deciphered by genome and transcriptome analyses. Nat. Genet. **44**:1060–1065. https://doi.org/10.1038/ng.2372.

Osbourn, A., Bowyer, P., Lunness, P., Clarke, B., and Daniels, M. (1995). Fungal pathogens of oat roots and tomato leaves employ closely related enzymes to detoxify different host plant saponins. Mol. Plant Microbe Interact. **8**:971–978. https://doi.org/10.1094/mpmi-8-0971.

Otomo, K., Kenmoku, H., Oikawa, H., König, W.A., Toshima, H., Mitsuhashi, W., Yamane, H., Sassa, T., and Toyomasu, T. (2004a). Biological functions of ent- and syn-copalyl diphosphate synthases in rice: key enzymes for the branch point of gibberellin and phytoalexin biosynthesis. Plant J. **39**:886–893. https://doi.org/10.1111/j.1365-313X.2004.02175.x.

Otomo, K., Kanno, Y., Motegi, A., Kenmoku, H., Yamane, H., Mitsuhashi, W., Oikawa, H., Toshima, H., Itoh, H., Matsuoka, M., et al. (2004b). Diterpene cyclases responsible for the biosynthesis of phytoalexins, momilactones A, B, and oryzalexins A-F in rice. Biosci. Biotechnol. Biochem. **68**:2001–2006. https://doi.org/10.1271/bbb.68.2001.

Pelot, K.A., Chen, R., Hagelthorn, D.M., Young, C.A., Addison, J.B., Muchlinski, A., Tholl, D., and Zerbe, P. (2018). Functional Diversity of Diterpene Synthases in the Biofuel Crop Switchgrass. Plant Physiol. **178**:54–71. https://doi.org/10.1104/pp.18.00590.

Phan, C.S., Li, H., Kessler, S., Solomon, P.S., Piggott, A.M., and Chooi, Y.H. (2019). Bipolenins K-N: New sesquiterpenoids from the fungal plant pathogen Bipolaris sorokiniana. Beilstein J. Org. Chem. **15**:2020–2028. https://doi.org/10.3762/bjoc.15.198.

Polturak, G., Dippe, M., Stephenson, M.J., Chandra Misra, R., Owen, C., Ramirez-Gonzalez, R.H., Haidoulis, J.F., Schoonbeek, H.J., Chartrain, L., Borrill, P., et al. (2022). Pathogen-induced biosynthetic pathways encode defense-related molecules in bread wheat. Proc. Natl. Acad. Sci. USA **119**:e2123299119. https://doi.org/10.1073/pnas.2123299119.

Prisic, S., Xu, M., Wilderman, P.R., and Peters, R.J. (2004). Rice Contains Two Disparate ent-Copalyl Diphosphate Synthases with Distinct Metabolic Functions. Plant Physiol. **136**:4228–4236. https://doi.org/10.1104/pp.104.050567.

Rosyara, U.R., Subedi, S., Duveiller, E., and Sharma, R.C. (2010). The effect of spot blotch and heat stress on variation of canopy temperature depression, chlorophyll fluorescence and chlorophyll content of hexaploid wheat genotypes. Euphytica **174**:377–390. https://doi.org/10.1007/s10681-010-0136-9.

Sarkar, D., Rovenich, H., Jeena, G., Nizam, S., Tissier, A., Balcke, G.U., Mahdi, L.K., Bonkowski, M., Langen, G., and Zuccaro, A. (2019). The inconspicuous gatekeeper: endophytic Serendipita vermifera acts as extended plant protection barrier in the rhizosphere. New Phytol. **224**:886–901. https://doi.org/10.1111/nph.15904.

Scheler, U., Brandt, W., Porzel, A., Rothe, K., Manzano, D., Božić, D., Papaefthimiou, D., Balcke, G.U., Henning, A., Lohse, S., et al. (2016). Elucidation of the biosynthesis of carnosic acid and its reconstitution in yeast. Nat. Commun. **7**:12942. https://doi.org/10.1038/ncomms12942.

Schmelz, E.A., Huffaker, A., Sims, J.W., Christensen, S.A., Lu, X., Okada, K., and Peters, R.J. (2014). Biosynthesis, elicitation and roles of monocot terpenoid phytoalexins. Plant J. **79**:659–678. https://doi.org/10.1111/tpj.12436.

Schmelz, E.A., Kaplan, F., Huffaker, A., Dafoe, N.J., Vaughan, M.M., Ni, X., Rocca, J.R., Alborn, H.T., and Teal, P.E. (2011). Identity, regulation, and activity of inducible diterpenoid phytoalexins in maize. Proc. Natl. Acad. Sci. USA **108**:5455–5460. https://doi.org/10.1073/pnas.1014714108.

Schneider, C.A., Rasband, W.S., and Eliceiri, K.W. (2012). NIH Image to ImageJ: 25 years of image analysis. Nat. Methods **9**:671–675. https://doi.org/10.1038/nmeth.2089.

Sekido, H., Endo, T., Suga, R., Kodama, O., Akatsuka, T., Kono, Y., and Takeuchi, S. (1986). Oryzalexin D (3, 7-Dihydroxy-(+)-sandaracopimaradiene), a New Phytoalexin Isolated from Blast-infected Rice Leaves. J. Pestic. Sci. **11**:369–372. https://doi.org/10.1584/jpestics.11.369.

Shimura, K., Okada, A., Okada, K., Jikumaru, Y., Ko, K.-W., Toyomasu, T., Sassa, T., Hasegawa, M., Kodama, O., Shibuya, N., et al. (2007). Identification of a Biosynthetic Gene Cluster in Rice for Momilactones. J. Biol. Chem. **282**:34013–34018. https://doi.org/10.1074/jbc.M703344200.

Tang, H., Wang, X., Bowers, J.E., Ming, R., Alam, M., and Paterson, A.H. (2008). Unraveling ancient hexaploidy through multiply-aligned angiosperm gene maps. Genome Res. **18**:1944–1954. https://doi.org/10.1101/gr.080978.108.

Thompson, J.D., Higgins, D.G., and Gibson, T.J. (1994). CLUSTAL W: improving the sensitivity of progressive multiple sequence alignment through sequence weighting, position-specific gap penalties and weight matrix choice. Nucleic Acids Res. **22**:4673–4680. https://doi.org/10.1093/nar/22.22.4673.

Tiedge, K., Li, X., Merrill, A.T., Davisson, D., Chen, Y., Yu, P., Tantillo, D.J., Last, R.L., and Zerbe, P. (2022). Comparative transcriptomics and metabolomics reveal specialized metabolite drought stress responses in switchgrass (Panicum virgatum). New Phytol. **236**:1393–1408. https://doi.org/10.1111/nph.18443.

Toruño, T.Y., Stergiopoulos, I., and Coaker, G. (2016). Plant-Pathogen Effectors: Cellular Probes Interfering with Plant Defenses in Spatial and Temporal Manners. Annu. Rev. Phytopathol. **54**:419–441. https://doi.org/10.1146/annurev-phyto-080615-100204.

Toyomasu, T., Shenton, M.R., and Okada, K. (2020). Evolution of Labdane-Related Diterpene Synthases in Cereals. Plant Cell Physiol. **61**:1850–1859. https://doi.org/10.1093/pcp/pcaa106.

Toyomasu, T., Usui, M., Sugawara, C., Kanno, Y., Sakai, A., Takahashi, H., Nakazono, M., Kuroda, M., Miyamoto, K., Morimoto, Y., et al. (2015). Transcripts of two ent-copalyl diphosphate synthase genes differentially localize in rice plants according to their distinct biological roles. J. Exp. Bot. **66**:369–376. https://doi.org/10.1093/jxb/eru424.

Toyomasu, T., Usui, M., Sugawara, C., Otomo, K., Hirose, Y., Miyao, A., Hirochika, H., Okada, K., Shimizu, T., Koga, J., et al. (2014). Reverse-genetic approach to verify physiological roles of rice phytoalexins: characterization of a knockdown mutant of OsCPS4 phytoalexin biosynthetic gene in rice. Physiol. Plant. **150**:55–62. https://doi.org/10.1111/ppl.12066.

Ube, N., Nishizaka, M., Ichiyanagi, T., Ueno, K., Taketa, S., and Ishihara, A. (2017). Evolutionary changes in defensive specialized metabolism in the genus Hordeum. Phytochemistry **141**:1–10. https://doi.org/10.1016/j.phytochem.2017.05.004.

Ube, N., Katsuyama, Y., Kariya, K., Tebayashi, S., Sue, M., Tohnooka, T., Ueno, K., Taketa, S., and Ishihara, A. (2021). Identification of methoxylchalcones produced in response to CuCl2 treatment and pathogen infection in barley. Phytochemistry **184**:112650. https://doi.org/10.1016/j.phytochem.2020.112650.

Urban, P., Mignotte, C., Kazmaier, M., Delorme, F., and Pompon, D. (1997). Cloning, Yeast Expression, and Characterization of the Coupling of Two Distantly Related *Arabidopsis thaliana* NADPH-Cytochrome P450 Reductases with P450 CYP73A5. J. Biol. Chem. **272**:19176–19186. https://doi.org/10.1074/jbc.272.31.19176.

Valente, M.T., Infantino, A., and Aragona, M. (2011). Molecular and functional characterization of an endoglucanase in the phytopathogenic fungus Pyrenochaeta lycopersici. Curr. Genet. **57**:241–251. https://doi.org/10.1007/s00294-011-0343-5.

Vandhana, T.M., Reyre, J.-L., Sushmaa, D., Berrin, J.-G., Bissaro, B., and Madhuprakash, J. (2022). On the expansion of biological functions of lytic polysaccharide monooxygenases. New Phytol. **233**:2380–2396. https://doi.org/10.1111/nph.17921.

Vaughan, M.M., Christensen, S., Schmelz, E.A., Huffaker, A., McAuslane, H.J., Alborn, H.T., Romero, M., Allen, L.H., and Teal, P.E. (2015). Accumulation of terpenoid phytoalexins in maize roots is associated with drought tolerance. Plant Cell Environ. **38**:2195–2207. https://doi.org/10.1111/pce.12482.

Wang, Q., Hillwig, M.L., and Peters, R.J. (2011). CYP99A3: functional identification of a diterpene oxidase from the momilactone biosynthetic gene cluster in rice. Plant J. **65**:87–95. https://doi.org/10.1111/j.1365-313X.2010.04408.x.

Wang, Q., Hillwig, M.L., Okada, K., Yamazaki, K., Wu, Y., Swaminathan, S., Yamane, H., and Peters, R.J. (2012a). Characterization of CYP76M5-8 indicates metabolic plasticity within a plant biosynthetic gene cluster. J. Biol. Chem. **287**:6159–6168. https://doi.org/10.1074/jbc.M111.305599.

Wang, Y., Tang, H., DeBarry, J.D., Tan, X., Li, J., Wang, X., Lee, T.-h., Jin, H., Marler, B., Guo, H., et al. (2012b). MCScanX: a toolkit for detection and evolutionary analysis of gene synteny and collinearity. Nucleic Acids Res. **40**:e49. https://doi.org/10.1093/nar/gkr1293.

Watanabe, M., Sakai, Y., Teraoka, T., Abe, H., Kono, Y., Uzawa, J., Kobayashi, K., Suzuki, Y., and Sakurai, A. (1990). Novel C19-Kaurane Type of Diterpene (Oryzalide A), a New Antimicrobial Compound Isolated from Healthy Leaves of a Bacterial Leaf Blight-resistant Cultivar of Rice Plant. Agric. Biol. Chem. **54**:1103–1105. https://doi.org/10.1080/00021369.1990.10870045.

Wawra, S., Fesel, P., Widmer, H., Timm, M., Seibel, J., Leson, L., Kesseler, L., Nostadt, R., Hilbert, M., Langen, G., and Zuccaro, A. (2016). The fungal-specific β-glucan-binding lectin FGB1 alters cell-wall composition and suppresses glucan-triggered immunity in plants. Nat. Commun. **7**:13188. https://doi.org/10.1038/ncomms13188.

Weber, E., Gruetzner, R., Werner, S., Engler, C., and Marillonnet, S. (2011). Assembly of Designer TAL Effectors by Golden Gate Cloning. PLoS One **6**:e19722. https://doi.org/10.1371/journal.pone.0019722.

Wilderman, P.R., Xu, M., Jin, Y., Coates, R.M., and Peters, R.J. (2004). Identification of Syn-Pimara-7,15-Diene Synthase Reveals Functional Clustering of Terpene Synthases Involved in Rice Phytoalexin/Allelochemical Biosynthesis. Plant Physiol. **135**:2098–2105. https://doi.org/10.1104/pp.104.045971.

Wu, D., Hu, Y., Akashi, S., Nojiri, H., Guo, L., Ye, C.-Y., Zhu, Q.-H., Okada, K., and Fan, L. (2022). Lateral transfers lead to the birth of momilactone biosynthetic gene clusters in grass. Plant J. **111**:1354–1367. https://doi.org/10.1111/tpj.15893.

Wu, Y., Zhou, K., Toyomasu, T., Sugawara, C., Oku, M., Abe, S., Usui, M., Mitsuhashi, W., Chono, M., Chandler, P.M., and Peters, R.J. (2012). Functional characterization of wheat copalyl diphosphate synthases sheds light on the early evolution of labdane-related diterpenoid metabolism in the cereals. Phytochemistry **84**:40–46. https://doi.org/10.1016/j.phytochem.2012.08.022.

Yadav, H., Dreher, D., Athmer, B., Porzel, A., Gavrin, A., Baldermann, S., Tissier, A., and Hause, B. (2019). Medicago TERPENE SYNTHASE 10 Is Involved in Defense Against an Oomycete Root

Pathogen. Plant Physiol. **180**:1598–1613. https://doi.org/10.1104/pp.19.00278.

Yakovlev, I., Vaaje-Kolstad, G., Hietala, A.M., Stefańczyk, E., Solheim, H., and Fossdal, C.G. (2012). Substrate-specific transcription of the enigmatic GH61 family of the pathogenic white-rot fungus Heterobasidion irregulare during growth on lignocellulose. Appl. Microbiol. Biotechnol. **95**:979–990. https://doi.org/10.1007/s00253-012-4206-x.

Zhang, J., Li, R., Xu, M., Hoffmann, R.I., Zhang, Y., Liu, B., Zhang, M., Yang, B., Li, Z., and Peters, R.J. (2021). A (conditional) role for labdane-related diterpenoid natural products in rice stomatal closure. New Phytol. **230**:698–709. https://doi.org/10.1111/nph.17196.

Zhou, K., Xu, M., Tiernan, M., Xie, Q., Toyomasu, T., Sugawara, C., Oku, M., Usui, M., Mitsuhashi, W., Chono, M., et al. (2012). Functional characterization of wheat ent-kaurene(-like) synthases indicates continuing evolution of labdane-related diterpenoid metabolism in the cereals. Phytochemistry **84**:47–55. https://doi.org/10.1016/j.phytochem.2012.08.021.

Westrick, N.M., Smith, D.L., and Kabbage, M. (2021). Disarming the host: detoxification of plant defense compounds during fungal necrotrophy. Front. Plant Sci. **12**:651716.